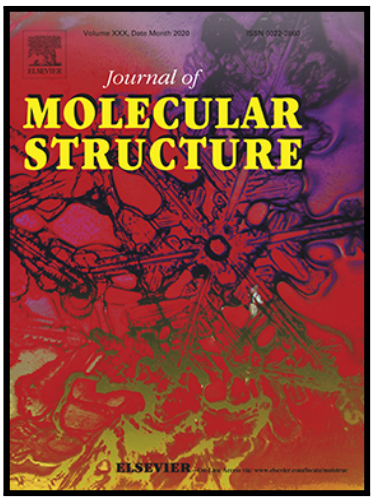

Synthesis, In Vitro Cytotoxic, Anti-Mycobacterium tuberculosis and Molecular Docking Studies of 4-Pyridylamino- and 4-(Ethynylpyridine)quinazolines

Kabelo B. Dilebo , Njabulo J. Gumede , Winston Nxumalo , Thabe M. Matsebatlela , Dikgale Mangokoana , Ngaoko R. Moraone , Bernard Omondi , Richard M. Mampa

PII: S0022-2860(21)00957-1
DOI: https://doi.org/10.1016/j.molstruc.2021.130824
Reference: MOLSTR 130824

To appear in: *Journal of Molecular Structure*

Received date: 30 October 2020
Revised date: 10 May 2021
Accepted date: 30 May 2021

Please cite this article as: Kabelo B. Dilebo , Njabulo J. Gumede , Winston Nxumalo , Thabe M. Matsebatlela , Dikgale Mangokoana , Ngaoko R. Moraone , Bernard Omondi , Richard M. Mampa , Synthesis, In Vitro Cytotoxic, Anti-Mycobacterium tuberculosis and Molecular Docking Studies of 4-Pyridylamino- and 4-(Ethynylpyridine)quinazolines, *Journal of Molecular Structure* (2021), doi: https://doi.org/10.1016/j.molstruc.2021.130824

Highlights:

- Successful synthesis of compounds of the series 4-chloro-, 4-(pyridylamino)- and 4-(ethynylpyridine)-quinazoline,
- Positive results from the Alamar Blue assay (*Mtb* H37Rv strain) which revealed promising MIC_{90} ranging from <0.7 to >125 µM and
- Candidate compounds were inductively docked into the 3ZXR enzyme and the more prominent hydrogen bond is between Nitrogen of the pyridine ring moiety of the **5** and **6** series with an OH group of SER280.
- A metal coordination between the methoxy benzene moiety of compounds in the **6** series and Mg^{2+} is also observed, explaining the SAR of these compounds to MtGS enzyme.

Synthesis, In Vitro Cytotoxic, Anti-*Mycobacterium tuberculosis* and Molecular Docking Studies of 4-Pyridylamino- and 4-(Ethynylpyridine)quinazolines

Kabelo B. Dilebo [1], Njabulo J. Gumede [2], Winston Nxumalo [1], Thabe M. Matsebatlela [3], Dikgale Mangokoana [3], Ngaoko R. Moraone [1], Bernard Omondi [4] and Richard M. Mampa[1,*]

[1] Department of Chemistry, University of Limpopo, Private Bag X1106, Sovenga 0727, South Africa; kbsebashe@gmail.com (K.B.D.); winston.nxumalo@ul.ac.za (W.N.); ngoakohitrj@gmail.com (N.R.M)

[2] Department of Chemistry, Mangosuthu University of Technology, Durban, P.O. Box 12363, Jacobs 4026, South Africa; Ngumede@mut.ac.za

[3] Department of Biochemistry, Microbiology and Biotechnology, School of molecular and Life Sciences, University of Limpopo, Private Bag X1106, Sovenga 0727, South Africa; thabem@ul.ac.za (T.M.M.); dikgalemangokoana@gmail.com (D.M.)

[4] School of Chemistry and Physics, University of KwaZulu-Natal, Pietermaritzburg Campus, Private Bag X01, Pietermaritzburg 3209, South Africa; Owaga@ukzn.ac.za

* Correspondence: richard.mampa@ul.ac.za; Tel.: +27 (015) 268 2334

Abstract: A series of 4-(pyridylamino)- and 4-(ethynylpyridine)quinazolines were successfully prepared via Sonogashira cross-coupling and dechloroamination reactions on the C(4)-Cl position of the requisite 2-(p-phenyl)-4-chloroquinazolines. The prepared compounds were characterized by means of ^{1}H- and ^{13}C-NMR, FT-IR and mass spectrometry techniques. The structure of 2-(4-chlorophenyl)-4-(2-(pyridin-4-yl)ethynyl)quinazoline from the 4-(ethynylpyridine) series was confirmed by single crystal X-Ray analysis which indicates monoclinic crystal system and P21/c space group. Compounds from the 4-chloro-, 4-(pyridylamino)- and 4-(ethynylpyridine)-quinazoline series were evaluated for anti-*Mycobacterium tuberculosis* (*Mtb*) properties in vitro employing rifampicin as a reference drug. The results from the Alamar Blue assay (*Mtb* H37Rv strain) revealed promising MIC_{90} ranging from <0.7 to >125 µM. The cytotoxicity of the synthesised compounds was tested against the Raw 264.7 microphage cell line at a maximum concentration of 50 µM. The possible mode of interaction against the *Mtb* was theoretically explained through molecular 3ZXR protein and the more prominent hydrogen bond is observed between the nitrogen of the pyridine ring moiety of the **5** and **6** series with OH group of SER280. Also, a metal coordination between the methoxy benzene moiety of compound **6e** and Mg^{2+} is also observed, explaining the SAR of these compounds to MtGS.

Keywords: *Mycobacterium tuberculosis*; quinazoline; glutamine synthetase; molecular docking; NMR; Sonogashira cross-coupling

1. Introduction

Tuberculosis (TB) is an infectious airborne disease that is caused by *Mycobacterium tuberculosis* [1]. According to the World Health Organisation (WHO), TB remains one of the most lethal diseases, with an emergence of about 10.4 million cases and 1.3 million deaths each year [2]. The advent of drug resistant TB strains and coexistence with Human Immunodeficiency Virus (HIV) worsens the situation [2]. Generally, treatment takes 6 to 9 months of chemotherapeutic regimen which includes a high dose of first-line drugs, isoniazid, ethambutol, rifampicin and pyrazinamide [2]. Failure to complete this treatment has led to the manifestation of multi-drug resistant (MDR) strains of the TB disease [2]. This resistance has undermined the chemotherapeutic effectiveness of the present drug regimen. The continued spread of TB is worrying despite 100% treatment success rate for normal TB strain followed by 50% of the MDR and 10% rate of extensively-drug resistant (XDR) strains amid extended period (up to 2 years) of treatment [2].

To this extent, TB drug candidates containing a quinazoline framework have been identified as potential building blocks for the development of new drugs owing to their wide range of biological properties [3]. Numerous quinazoline derivatives are known to exhibit anticancer, antimalarial, antiviral, anti-inflammatory and antibacterial properties [4–7]. Some of these quinazoline derivatives have been reported to inhibit the proliferation of MDR and XDR TB strains [8]. The 2-(3-Fluorophenyl)-4-oxoquinazolin-3(4*H*)-yl-3-fluorobenzoate (**A**) shown in Figure **1** for example, was found to inhibit several clinical isolates of MDR and XDR TB by exhibiting MIC_{90} values of 6.5 – 6.6 µM. In addition, enzyme kinetics and molecular docking studies suggested that the compound is capable of binding branched-chain amino acids (BCAAs)

biosynthetic pathway promoter's i.e. acetohydroxyacid synthase (AHAS) and serine-threonine protein kinases (STPKs) of glutamine synthetase [9, 10]. Glutamine synthetase, which is an enzyme responsible for the catalysis of ATP-dependent condensation of ammonium and L-glutamate at the amino acid binding site resulting in the formation of glnA1, is essential for the growth of *Mtb* in both *in vitro* and *in vivo* [10]. A disturbance at the amino acid binding site stops cell wall biosynthesis leading to cell death [10]. Likewise, Gising and coworkers designed and synthesised trisubstituted imidazole (**B**) derivatives represented in Figure **1** bearing heterocyclic and pyridyl substituents which were found to bind and inhibit the activity of glutamine synthetase with IC_{50} values of 2.2 ± 0.3 µM to >25 µM [11]. Similarly, Nordqvist and coworkers prepared imidazo[1,2-a]pyridine-based derivatives (**C**) (Figure **1**) which were found to exhibit IC_{50} of 3.0 ± 0.1 µM to >25 µM against glutamine synthetase [12]. Based on this literature precedence, it was envisaged that the 4-Pyridylamino- and 4-(Ethynylpyridine)quinazolines would also represent additional agents which may target and inhibit the activity of glutamine synthetase.

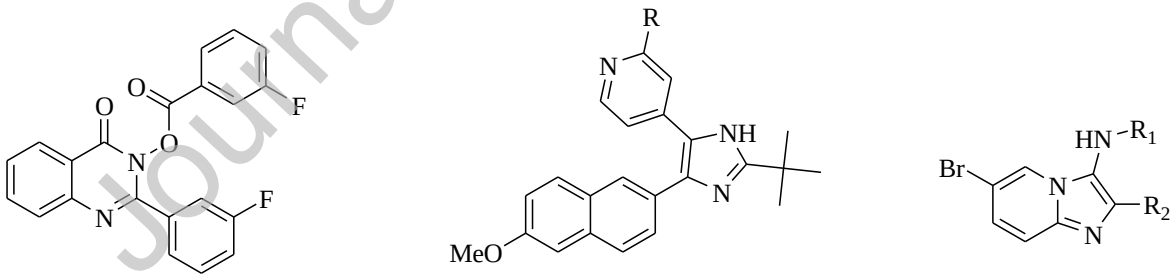

A **B** **C**

Figure 1: Structures of potential inhibitors of glutamine synthetase of *Mycobacterium tuberculosis*

In this study, we focus on the synthesis and functionalisation of prerequisite 4-chloro-quinazolines on the *C(4)* position to generate novel pyridylquinazoline derivatives. In addition,

in vitro anti-*Mtb* screening and cytotoxicity studies of the newly synthesised compounds were performed and complemented by computational molecular docking studies to evaluate the possible binding to the target enzyme, glutamine synthetase (PDB: 1HTO, 3ZXR, and 3ZXV).

2. Results

2.1. *Chemistry*

2.1.1. Synthesis of 2-Aryl-quinazolin-4(3*H*)-ones **3a**–**3e** and 2-Aryl-4-chloroquinazolines **4a**–**4e**

The first step involves the synthesis of 2-aryl-quinazolin-4(3*H*)-ones **3a**–**3e** to be used as substrates for the requisite 2-aryl-4-chloroquinazolines **4a**–**4e**, which is reported in the literature [13–16], Oxidative one-pot cyclocondensation reaction of anthranilamide **1a** with *para*-substituted benzaldehyde derivatives **2a**–**2e** in the presence of molecular iodine (2 equiv.) in ethanol at 80 °C led to the desired 2-aryl-quinazolin-4(3*H*)-ones **3a**–**3e** as indicated in Scheme 1. The 2-aryl-quinazolin-4(3*H*)-ones 3a–**3e**, were obtained in high yields (greater than 86%, Table 1) following a modified literature method [16] and characterised using ^{1}H-NMR, ^{13}C-NMR and FT-IR spectroscopic techniques. The ^{1}H-NMR spectra of compounds **3a**–**3e** revealed the presence of a broad singlet at 12.75 ppm corresponding to the N-H proton of the α-nitrogen. Furthermore, protons in the aromatic region ranging from 7.53–8.20 ppm are assigned to the 2-aryl substituent and the quinazoline backbone. The amide nature of the compounds was confirmed by FT-IR spectroscopy due to the presence of C-N and C=O in the regions v_{max} 1531–1583 cm^{-1} and v_{max} 1656–1691 cm^{-1}, respectively.

The next step was to generate an electrophilic centre at the *C4*-position of the 2-aryl-quinazolin-4(3*H*)-ones scaffolds **3a**–**3e** through oxidative aromatisation to afford 2-aryl-4-

chloroquinazolines **4a**–**4e** (Table 1). The 2-aryl-quinazolin-4(3*H*)-ones **3a**–**3e** in DMF solution was treated with excess thionyl chloride following a literature method to afford 2-aryl-4-chloro-quinazolines **4a**–**4e** [16]. The reaction was driven to completion by refluxing at 80 °C for 2 h. The full conversion of the starting materials was confirmed by the absence of an N-H signal from the ^{1}H-NMR spectra of the 2-aryl-4-chloro-quinazolines **4a**–**4e**, also indicated in Scheme 1. The FT-IR spectra of compounds **4a**–**4e** revealed the absence of the C=O stretch, thus confirming successful formation of the *C(4)-Cl* bond.

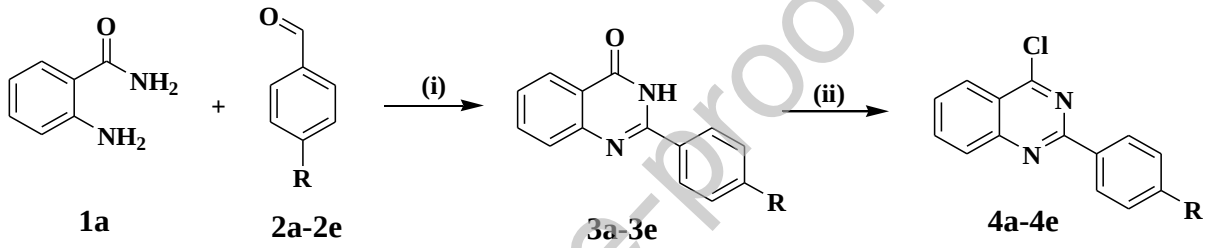

Scheme 1. Synthesis of 2-aryl-quinazolin-4(3*H*)-ones **3a**–**3e** and 2-aryl-4-chloro-quinazolines **4a**–**4e**. *Reagents and conditions*: (i) I_2, 80 °C, EtOH, 6 h; (ii) $SOCl_2$, DMF, 80 °C, 2 h. **R** = -Cl, -Br, -F, -NO_2 and -OMe

Table 1. Yields of compounds **3a**–**3e** [13] and **4a**–**4d** [14], **4e** [15].

Compound	%Yield(R)	Compound	%Yield(R)
3a	87 (-Cl)	**4a**	88 (-Cl)
3b	91 (-Br)	**4b**	93 (-Br)
3c	93 (-F)	**4c**	90 (-F)

3d	90 (-NO_2)	**4d**	84 (-NO_2)
3e	93 (-OMe)	**4e**	89 (-OMe)

2.1.2. Amination of **4a**–**4e** with 2-Amino-3-nitropyridine

The synthesis of 2-aryl-*N*-(3-nitropyridin-2-yl)quinazolin-4-amine **5a**–**5e** was achieved through a slight modification of a literature procedure [17]. The Paumo et al. [17] procedure employs a combination of THF-*i*-PrOH and HCl which protonates the *N*-1 position of the 4-chloroquinazolines and renders the heterocyclic ring electron deficient and *C*-4 more electrophilic. Based on this observation, we employed 2-amino-3-nitropyridine and the 2-aryl-4-chloroquinazolines following the same conditions as in the literature procedure, unfortunately only trace amounts of the desired product were achieved. The reason for the low yield was attributed to the poor solubility of 2-amino-3-nitropyridine in the solvent mixture used, i.e. THF-*i*-PrOH. Therefore, in order to improve the solubility, a mixture of THF-DMF (3:1) with 98% sulfuric acid serving as a catalyst was applied to afford 2-aryl-*N*-(3-nitropyridin-2-yl)quinazolin-4-amine derivatives **5a**–**5e** (Scheme 2) in high yields (Table 2). The successful synthesis of compounds **5a**–**5e** was confirmed by ^{1}H-NMR, ^{13}C-NMR, FT-IR spectroscopy and HRMS spectroscopic techniques, all included in the Supplementary Material as Figures s1 to s15. The ^{1}H-NMR spectra showed the appearance of an N-H signal at around 12.60 ppm, with protons from the nitropyridyl ring showing multiplicities of doublet of doublets, doublet and a multiplet ranging from 6.73 ppm to 8.40 ppm in the aromatic region. The ^{13}C-NMR spectra showed the quaternary carbon of the nitro-deshielded group resonating at around 149.00 ppm. The presence

151 of the N-H group was confirmed by a broad N-H stretch in the region 3461–3464 cm^{-1} on FT-IR

152 spectra.

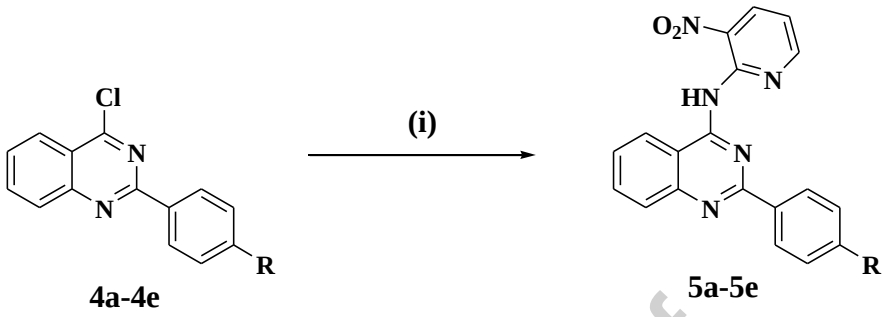

153

154 **Scheme 2.** Amination of **4a**–**4e** with 2-amino-3-nitropyridine. *Reagents and conditions*:

155 (i) 2-NH_2-3-$NO_2C_5H_3N$, 98% sulfuric acid, 65 °C, 5 h.

156 **Table 2.** Yields of compounds **5a**–**5e**.

Compound	R	% Yield
5a	-Cl	95
5b	-Br	78
5c	-F	92
5d	-NO_2	66
5e	-O-Me	84

157 2.1.3. Sonogashira-Cross Coupling of **4a**–**4e**

158 The first attempt following Sonogashira cross-coupling conditions of the 2-aryl-4-chloro-
159 quinazolines **4a**–**4e** at the *C(4)-Cl* position using $Pd(PPh_3)_4$, CuI, Et_3N and 1.5 equiv. of 4-
160 ethynyl-pyridine hydrochloride in dry THF at mild temperatures (40–60 °C) was unsuccessful,
161 and only the starting materials (4-ethynylpyridine and 4-chloroquinazolines) were isolated. Air
162 and moisture sensitivity of the Pd(0) source, tetrakis(triphenylphosphine)palladium(0) was
163 attributed as contributing to the failure of Sonogashira cross-coupling in this case. In the second
164 attempt, the Pd(0) source was replaced with $PdCl_2(PPh_3)_2$ whilst keeping other reagents constant
165 but this procedure also led to the recovery of starting materials. Further attempts in high boiling
166 solvents such as DMF and dioxane also proved unsuccessful. Generally, the Sonogashira
167 reaction requires a nucleophilic terminal alkyne which reacts with a CuX (X = Br, I) salt and
168 successively gives a copper acetylide [18]. The failure of the second attempt using Et_3N, was
169 attributed to the basic conditions not being favourable for deprotonating the hydrochlorinated 4-
170 ethynlpyridine substrate. Consequently, trace amounts of our desired product was obtained when
171 using K_2CO_3, Na_2CO_3 and NaOH as our base during coupling. Since the Sonogashira cross-
172 coupling reaction mechanism requires a relatively strong base to deprotonate the terminal
173 acetylene, we then opted for Cs_2CO_3 [16]. In a one-pot reaction synthesis, 4-chloro-2-(4-
174 chlorophenyl)quinazoline (**4a**, 1 equiv.) was reacted with $PdCl_2(PPh_3)_2$ (10%), CuI (10%) and
175 Cs_2CO_3 (2 equiv.) in 3:1 THF-water and the reaction was left to stir for 24 h under at mild heat
176 (40–60 °C) under N_2 to produce a 98% yield of **6a** (Table 3) after recrystalisation from diethyl
177 ether, as indicated in Scheme 3. Synthesis of derivatives **6b**–**6e** followed that of **6a** while varying
178 the *para*-position of the 2-aryl group (Table 3). Successful synthesis of **6a**–**6e** was confirmed
179 using ^1H, ^{13}C-NMR, FT-IR spectroscopy and HRMS spectroscopic techniques (see Figures s16

to **s30** in the Supplementary Information). The ^{1}H-NMR showed two additional doublet peaks resonating at 7.60 and 8.74 ppm. The ^{13}C-NMR spectra showed carbons of the π-spacer (C≡C) resonating at 88.22 and 93.71 ppm. Further characterisation using FT-IR spectroscopy showed the presence of *Csp-Csp* band at v_{max} 2219.44 cm^{-1}. The HRMS (ESI+) revealed *m*/*z* M+ and M2+ molecular ion peaks due to the presence of chlorine isotopes 35 and 37 for **6a** and bromine isotopes 79 and 81 for **6b** (see HRMS spectra as Figures s18 and s21 for **6a** and **6b**, respectively in the Supplementary Information).

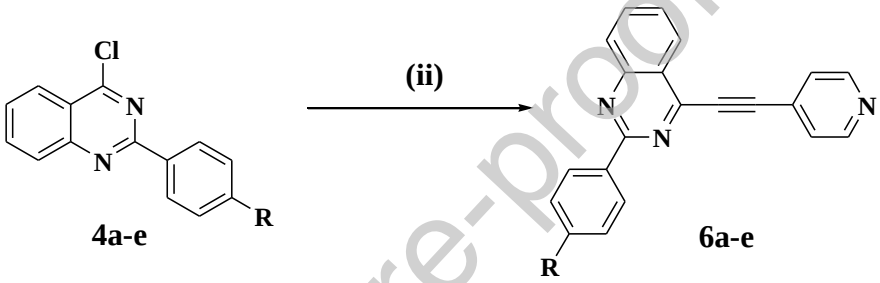

Scheme 3. Sonogashira cross-coupling with 4-ethynylpyridine. *Reagents and solutions*: (ii) 4-ethynylpyridine hydrochloride, $PdCl_2(PPh_3)_2$, CuI, Cs_2CO_3, THF-water, 60 °C, 24 h.

Table 3. Yields of compounds **6a**–**6e**.

Compound	R	% Yield
6a	-Cl	98
6b	-Br	90

6c	-F	94
6d	-NO_2	94
6e	-OMe	79

2.2. *Crystal Structure Interpretation*

The solid-state geometry of 4-(ethynylpyridine)quinazolines **6a**–**6e** was established by means of single-crystal X-ray diffraction (XRD). Crystals of compound **6a** were grown by slow evaporation of a chloroform/hexane solution. The crystal data and structure refinement for compound **6a** are shown in Table 4. The molecular structure of compound **6a** is given in Figure 2 and the selected bond distances and angles are included in Table 5.

Table 4. Crystal data and structure refinement for compound **6a**.

Identification code	Shelx
Empirical formula	$C_{21}H_{12}ClN_3$
Formula weight	341.79
Temperature	100(2) K
Wavelength	0.71073 Å
Crystal system	Monoclinic
Space group	P 21/c

Unit cell dimensions	a = 3.8537(5) Å	α = 90°
	b = 21.924(3) Å	β = 93.536(6)°
	c = 18.377(2) Å	γ = 90°
Volume	1549.7(3) $Å^3$	
Z	4	
Density (calculated)	1.465 Mg/m^3	
Absorption coefficient	0.254 mm^{-1}	
F(000)	704	
Crystal size	0.600 × 0.040 × 0.040 mm^3	
Theta range for data collection	1.447 to 26.661°	
Index ranges	$-4 \le h \le 4$, $-27 \le k \le 27$, $-23 \le l \le 23$	
Reflections collected	24266	
Independent reflections	3227 [R(int) = 0.0367]	
Completeness to theta = 25.242°	0.992	
Refinement method	Full-matrix least-squares on F2	
Data / restraints / parameters	3227 / 0 / 226	
Goodness-of-fit on F^2	1.16	
Final R indices [I > 2sigma(I)]	R1 = 0.0490, wR2 = 0.1162	
R indices (all data)	R1 = 0.0583, wR2 = 0.1204	
Extinction coefficient	n/a	
Largest diff. peak and hole	0.570 and −0.271 $e.Å^{-3}$	

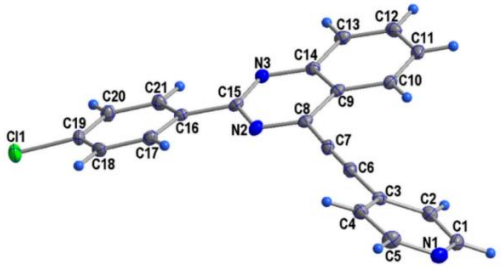

200 **Figure 2.** Crystal structure of compound **6a**.

201 **Table 5**. Selected bond distances (Å), bond angles (°) and dihedral angles (°).

Bond Distances (Å)	
C(3)-C(6)	1.433(3)
C(6)-C(7)	1.194(3)
C(7)-C(8)	1.442(3)
C(8)-N(2)	1.318(3)
C(15)-N(3)	1.323(3)
C(14)-N(3)	1.362(3)
C(19)-Cl(1)	1.746(2)
C(1)-N(1)	1.335(3)
C(5)-N(1)	1.344(3)
Bond angles (°)	
C(15)-C(16)-C(21)	120.4(2)
C(15)-C(16)-C(17)	120.7(2)
C(7)-C(8)-N(2)	118.1(2)
C(3)-C(6)-C(7)	175.8(2)
Dihedral angles (°)	

C(3)-C(6)-C(7)-C(8)		-13(5)

The molecule crystallises with one molecule in the asymmetric unit. The molecule contains a quinazoline moiety, a 4-ethynylpyridine moiety and a chlorobenzene ring, all which define three sets of planes. The 4-chlorobenzene ring, the 4-ethynylpyridine moiety and the quinazoline moiety planes are not co-planar. This phenomenon has been observed in related compounds from literature [19,20]. The dihedral angles between the chlorobenzene ring and the 4-ethynylpyridine moiety is 12.67(6)°, that between the 4-ethynylpyridine moiety and the quinazoline moiety is 35.33(6)° while that between chlorobenzene ring and 4-ethynylpyridine 37.58(6)°. In the crystal, the molecules are stabilized via a C—H…N intermolecular interactions (C…N = 2.7881(4) Å and <C—H…N = 100°) and a strong π…π intermolecular interactions between adjacent quinazoline moieties (Cg…Cg = 3.6034, symmetry code = 1- x, -y, -z).

2.3. *Biological Evaluation*

2.3.1. In Vitro Anti-Mycobacterium Tuberculosis Activity

Pyridine containing compounds serve a great purpose in inhibiting the progression of *Mtb* cells [21]. Such derivatives are represented by a small commercially available first-line drug isoniazid and the second-line drugs ethionamide and prothionamide [22,23]. The conjugated π-system of the pyridine ring is reported to bring about receptor π-π intermolecular interactions and hydrogen bond interaction through the sp^2-hybridised nitrogen [24]. Accordingly, in vitro anti-*Mycobacterium tuberculosis* activity of compounds **4a**–**4e**, **5a**–**5e** and **6a**–**6e** were assayed against the $H_{37}Rv$ strain in the concentration range of 0.723–125 µM according to the procedure explained in Section 3.6. Activity was assessed at MIC_{90}, which is the minimum concentration

223 required to inhibit at least 90% of the bacterial population, employing rifampicin as a reference
224 drug. As an aid for structural activity relationship (SAR) analysis, compounds which exhibited
225 MIC_{90}, ≤10 µM were rendered active (relative to rifampicin, Table 6); compounds with MIC_{90}
226 ranging from 10–25 µM were considered to have moderate activity; MIC_{90} ranging from 25 µM–
227 (>125 µM) was considered as poor activity. Consequently, a structure activity relationship
228 (SAR) study was explored on the 4-position of the quinazoline scaffold and the 4-position of the
229 2-aryl substituents. Firstly, the 4-chloroquinazolines **4a**–**4e** were tested against *Mtb* H_{37}Rv strain
230 and no significant activity was observed (MIC_{90}, >125 µM). We then hypothesised that the poor
231 activity was attributed to the poor solubility of these compounds **4a**–**4e** in DMSO. To improve
232 the solubility, a 3-nitropyridylamino group was introduced on the *C(4)* position of the 4-
233 chloroquinazolines. Introduction of the amine group resulted in moderate improvement in
234 activity for compounds **5b**–**5e**, with MIC_{90} ranging from 20.65–109.09 µM. Another contributing
235 factor was hypothesised to be the presence of the -NO_2 group ortho to the amine group. This is
236 true because the -NO_2 group is reported to enhance anti-*Mtb* activity, as it binds –NH groups of
237 amino acids found in active sites of *Mtb* proteins [21]. A second pyridine moiety, 4-
238 ethynylpyridine, introduced at the *C(4)* position led to significant improvement in potency, with
239 MIC_{90} ranging from <0.72 µM–23 µM for compounds **6a**–**b** and **6d**–**6e**.

240 From both series of **5a**–**5e** and **6a**–**6e**, compounds **5e** and **6e**, both containing a methoxy
241 group on the *para* position of the 2-aryl substituent appeared to show good potency with MIC_{90}
242 of 20.65 µM and <0.72 µM, respectively. This moderate to significantly higher activity was
243 hypothesised to be due to the presence of the polar effect of the methoxy oxygen which is
244 responsible for hydrogen bonding during inhibition (see Figure 2). Other compounds with good
245 activity emanated from the **6a**–**6e** series i.e. compounds **6a** and **6b**, MIC_{90}, 9.82 µM and 9.39

246 µM, respectively. Apart from the biologically influential π-conjugated system of the pyridine
247 ring, these two compounds contain halogen groups i.e. 4-Cl and 4-Br, which are responsible for
248 halogen bond interactions probably with amino acids in the active site of *Mtb* proteins (see
249 Figure 2 and Figure 3). Compounds bearing the 4-ethynylpyridine demonstrated better activity as
250 compared to compounds with 3-nitropyridylamino group, as evident when comparing **6a** vs **5a**,
251 **6b** vs **5b**, **6d** vs **5d**, and **6e** vs **5e**. An exception was noted for compounds **6c** vs **5c** where the
252 introduction of an ethynylpyridine resulted in loss of activity.

253

254

255

256 Compounds **6a**–**6e** were further evaluated for their in vitro cytotoxic effects against Raw
257 264.7 microphage cells using a Glomax-Multi microplate reader MTT assay. The lethal dosage
258 of the compounds was recorded as IC_{50} (which is the inhibitory concentration required to inhibit
259 50% of viable cells) at a maximum concentration of 50 µM. All assayed compounds showed low
260 cytotoxicity against the microphages i.e. $IC_{50} > 50$ µM (**Table 6**). The low cytotoxicity of these
261 compounds allowed for further investigations of crucial efficacy determining parameters such as
262 the selectivity index (SI) ratio. The selectivity index ratio is an acceptable parameter responsible
263 for measuring the gap between cytotoxicity and anti-mycobacterial activity [25]. Theoretically,
264 the higher the SI ratio, the more effective and safer a drug would be during in vivo treatment for
265 bacterial infection. According to literature [25], the SI ratio should be ≥10 for compounds to be
266 considered as new drug leads. A compound's SI ratio means that, the compounds are cytotoxic
267 only at high concentrations and show anti-*Mtb* activity at lower concentrations. Accordingly,

268 selectivity index ratios for compounds **6a**–**6e** were calculated as SI = IC_{90}/ MIC_{90}. In this study,
269 only compounds **6b** and **6e** suited the literature SI window with SI ratios of 12.16 and >150.24
270 respectively (Table 6).

271 **Table 6.** Anti-mycobacterial activity (MIC_{90} in µM) of compounds **4a**–**4e**, **5a**–**5e** and **6a**–**6e**.

Compound Structure	Entry Number	R	Compound ID	MIC_{90} (µM)	IC_{50}	SI
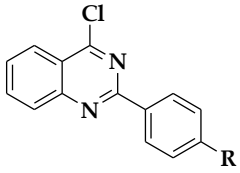	1	-Cl	**4a**	>125	ND	ND
	2	-Br	**4b**	>125	ND	ND
	3	-F	**4c**	>125	ND	ND
	4	$-NO_2$	**4d**	>125	ND	ND
	5	-OMe	**4e**	>125	ND	ND
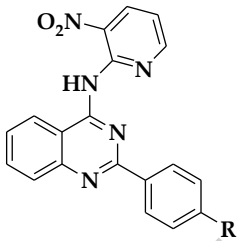	6	-Cl	**5a**	>125	ND	ND
	7	-Br	**5b**	40.84	ND	ND
	8	-F	**5c**	85.71	ND	ND
	9	$-NO_2$	**5d**	109.09	ND	ND
	10	-OMe	**5e**	20.65	ND	ND
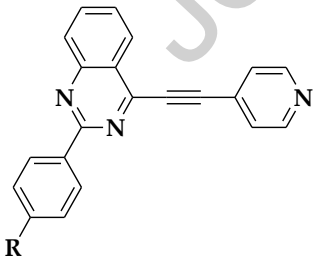	11	-Cl	**6a**	9.82	51.30	5.22
	12	-Br	**6b**	9.39	114.17	12.16
	13	-F	**6c**	>125	52.36	ND
	14	$-NO_2$	**6d**	23.46	59.04	2.52
	15	-OMe	**6e**	<0.72	108.17	>150.24
Rifampicin				0.12		

ND = Not determined

2.3.2. Molecular Docking Studies

The accuracy of docking experiments were measured by performing cross-docking of compound **2** and **3** (compound numbers taken as represented from Gising et al [11]) co-crystallized to x-ray crystal structures 3ZXV and 3ZXR, respectively. These two co-crystallized structures were designed by Gising et al [11], and were tested against Mycobacterium tuberculosis glutamine synthetase (MtGS) enzyme both in vitro and in silico. There is a huge body of evidence in the literature postulating that the accuracy of docking results is system dependent [26,27]. Also, docking results are only able to correctly discriminate between compounds which bind to the receptor and those that do not show any affinity to the target receptor correctly, as previously reported by both Graves et al. and Mobley et al. [28,29]. Hence, methods such as MMGBSA (Kollman et al [30]), MMPBSA (Kuhn et al. [31]) and recently water map score (Robinson et al. [32]), and Free Energy Perturbation (FEP+) (Ciordia et al. [33]) have been developed and used successfully by various academic groups and some big pharma companies to overcome this shortcoming. The relative binding affinities from FEP+ can be correctly correlated with in vitro (experimental) values, a recent focus in molecular modeling. However, in this work only docking by virtue of cross-docking and classical Glide XP docking were employed.

This approach is aimed at using docking to establish the binding mechanism of the candidate compounds designed, and their ability to block the biosynthesis of poly-L-glutamate−glutamine by MtGS. In comparison to compound **2** and **3** designed by Gising et al. Figure 3 shows the cross-docking poses of compound **2** and **3** from Gising et al [11], overlaid on the native conformers of the x-ray crystallographic structures of MtGS. Figure 3a shows an

overlay of **2** (RMSD of 1.34Å) on the native conformer; and the binding mode is not correctly reproduced. A conformational change is evident on **2** when cross-docked with 3ZXV. However, in Figure s27a classical Glide XP docking of **2** to 3ZXR reproduces the native conformation of **2** on the x-ray crystal structure (3ZXV). The more prominent hydrogen bond is between Nitrogen of the pyridine ring moiety of **2** and the OH group of SER280. Also, a hydrogen bond between the NH_2 group of the pyridine moiety and the carbonyl group of LYS361 is observed. Gising et al [11], also observed the same binding mode and similar hydrogen bonds.

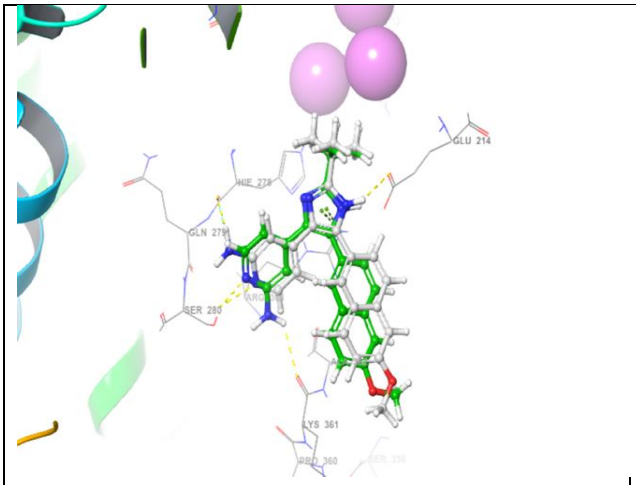

(a)

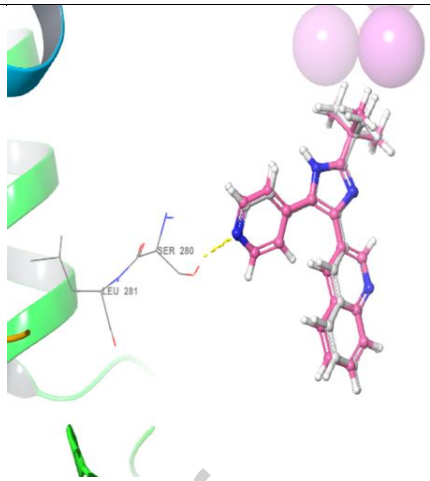

(b)

Figure 3. (a) The cross-docking pose of Compound **2** (grey carbons) overlay to the native conformer (green carbons) from the co-crystalized structure of MtGS PDB ID (3ZXV), with an RMSD of 1.34 Å. Mg^{2+} ions are shown in purple spheres. **(b)** The cross-docking pose of Compound **3** (pink carbons) overlay to the native conformer (grey carbons) from the co-crystalized structure of MtGS PDB ID (3ZXR), with an RMSD of 0.28 Å.

The cross-docking of compound **3** on 3ZXR is shown in Figure 3 (b), the bound conformation of **3** and the native co-crystalized structure of **3** overlays perfectly with an RMSD of 0.28 Å. SER280 hydrogen bonds with the Nitrogen atom of the pyridine ring of **3**. Furthermore, figure s27b has revealed that classical Glide XP is able to reproduce the native bound conformation of **3** to MtGS (3ZXR). The binding mode and the hydrogen bond observed in figure 3b and s27b are consistent with those observed by Gising et al [11].

We further cross-docked AMP co-crystalized with MtGS from PDB ID 1HTO. AMP was not well superposed over the native conformer resulting in an RSMD of 2.24Å (see Figure 4a). Then, AMP was further docked on 3ZXR using classical Glide XP.

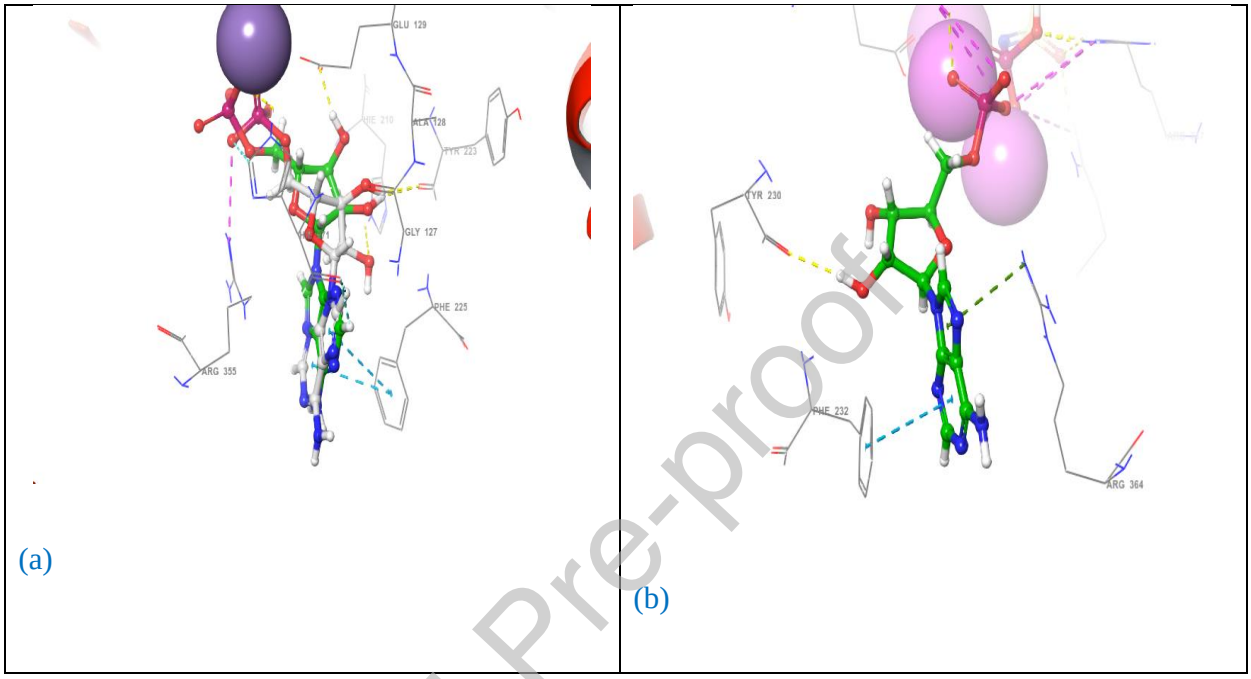

Figure 4. **(a)** AMP in the native conformation (grey carbons) and is not well overlaid with cross-docked conformation (green carbons) into the active site cavity of 1HTO. Manganese 2+ ion is shown as dark purple spheres. **(b)** AMP (green carbons) bound to amino acids of 3ZXR, Magnesium 2+ ions are shown as light purple spheres.

It is evident that the binding mode of AMP to 1HTO and 3ZXR is not the same and the active site cavities are quite different including cofactors such as manganese (1HTO) and magnesium (3ZXR). The evidence observed above, thus validates 3ZXR as an x-ray crystal structure of choice for further studies.

Molecular docking has been previously used successfully as a computer-aided drug design (CADD) method for the design of *Mycobacterium tuberculosis* drug candidates [11].

Docking of compounds **5a**–**5e**, **6a**–**6e** was performed by using classical Glide XP docking on 3ZXR enzyme. Induced Fit Docking (IFD) did not reproduce the native poses, thus indicating that the binding of these compounds understudy including compounds **2** and **3** from Gising et al follows a lock and key approach. Therefore, IFD was not used for further studies.

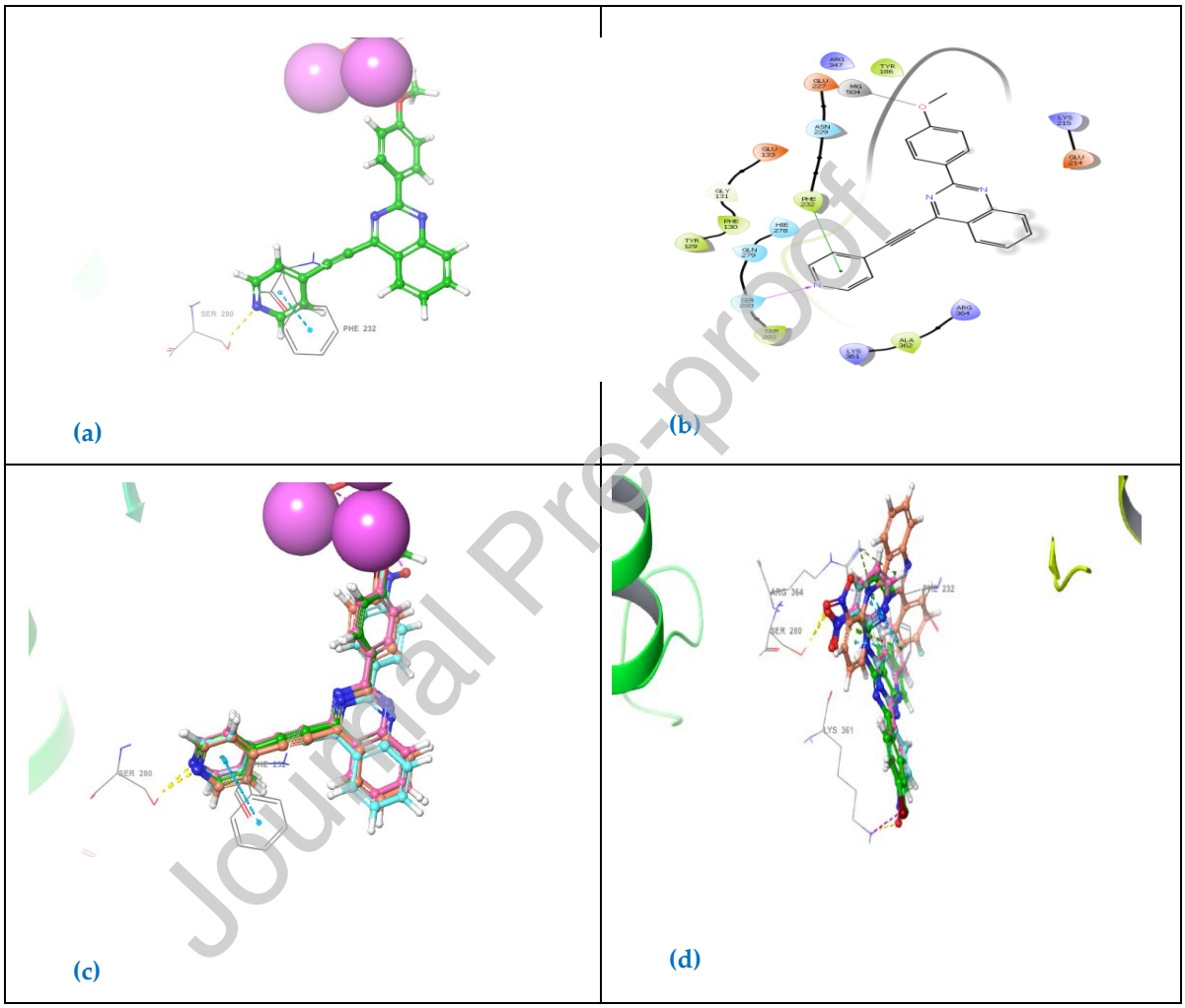

Figure 5. (**a**) IFD binding pose of **6e** in the active site cavity of 3ZXR depicting the hydrogen bonds, and π-π interactions. (**b**) Ligand interaction diagram of **6e** with important amino acid residues in the active site cavity of 3ZXR and a metal coordination of methoxy benzene moiety and Mg^{2+}. **(c)** An overlay of compounds in the

6 series, including **6e** (green carbons), **6c** (pink carbons), **6d** (light blue carbons), and **6b** (light brown carbons). **(d)** An overlay of compounds in the **5** series, including **5a** (green carbons), **5b** (pink carbons), **5c** (light blue carbons), and **5d** (light brown carbons).

The Glide XP docking results have revealed the binding mode of compound **6e** to MtGS enzyme, that is facilitated by a hydrogen bond between SER280 and the Nitrogen atom of the pyridine ring moiety of **6e**. A π-π interaction between the pyridine ring of **6e** and the benzene ring of PHE232 is shown (see Fig. 5a). Furthermore, a metal coordination between the Oxygen atom of the methoxybenzene moiety of **6e** and Mg^{2+} ion of MtGS is shown (see Fig. 5b). The binding modes of the compounds in the **6** series is similar to the binding mode observed by Gising et al [11]. Also, the validation of the docking by cross-docking follows the same binding mechanism. This therefore, proves that the compounds in the **6** series are MtGS inhibitors.

Compounds in the **5** series, on the other hand, have revealed a different binding mode hypothesis. They prefer to locate themselves far below the Mg^{2+} ions moiety, the Oxygen of the nitropyridine ring hydrogen bonds with SER280. Also, some π-π interactions between the compounds in the **5** series and PHE232 and ARG364 are shown see Fig. 5d. The classical Glide XP method employed in this work has been able to assist in determining compounds that would be bio-active prior to synthesis and biological evaluations. It is worth noting that compounds that were synthesized without being tested in silico for their bioactivity exhibited no activity towards the enzyme such as compounds in the **3a**–**3e** and **4a**–**4e** series.

2.3.3. Calculated Physicochemical and ADME Properties

The predicted physicochemical and ADME properties using QikProp v5.7 [34] for compounds in the **5a**–**5e** and **6a**–**6e** series are presented in Table 8. In particular, the predicted

central nervous system activity (CNS), octanol/gas partition coefficient (logPo/w), aqueous solubility (logS), IC_{50} value for blockage of HERG K+ channels (logHERG), brain/blood partition coefficient (logBB), and human oral absorption (%Human Oral Absorption). It is worth noting that only compound **6b** violated the Lipinski's rule of 5 by having an aqueous solubility <6.5. The predicted physicochemical properties have revealed that the most potent compound **6e** is drug-like and does not violate the Lipinski's rule of 5. In fact, all the compounds in the series are drug-like, with an exception of compound **6b**.

Table 7. Predicted physicochemical and ADME properties for compound **5a**–**5e** and **6a**–**6e** series**.**

Molecule ID	CNS [a]	MW [b]	logPoct [c]	logPw [d]	logPo/w [e]	logS [f]	CIlogS [g]	logHERG [h]	PCaco [i]	LogBB [j]	#metab [k]	LogKhsa [l]	%Human Oral Absorption [m]
6b	1	386.250	16.005	7.997	5.385	−6.562	−6.971	−7.398	3,712.551	0.096	2	0.754	100.000
6d	-2	352.351	17.624	9.358	4.052	−5.739	−5.787	−7.396	439.440	−1.200	3	0.505	100.000
6c	1	325.34	15.448	8.008	5.027	−6.031	−5.677	−7.336	3,712.716	0.030	2	0.647	100.000

		4											
6a	1	341.799	15.890	7.988	5.267	−6.420	−6.027	−7.370	3,712.415	0.084	2	0.729	100.000
6e	0	337.380	15.848	8.454	4.860	−5.817	−5.585	−7.342	3,706.216	−0.153	3	0.576	100.000
5a	0	377.789	17.524	10.079	4.354	−5.783	−6.414	−6.655	965.137	−0.568	3	0.559	100.000
5e	-1	373.370	17.664	10.546	3.922	−5.257	−6.025	−6.634	967.645	−0.805	4	0.450	100.000
5b	0	422.240	17.676	10.098	4.432	−5.917	−7.327	−6.702	950.905	−0.568	3	0.585	100.000
5d	-2	388.342	18.883	11.453	3.165	−5.227	−6.229	−6.700	114.154	−1.810	4	0.397	82.302
5c	0	361.334	17.083	10.105	4.095	−5.418	−6.077	−6.617	953.021	−0.621	3	0.487	100.000

[a] Predicted central nervous system activity, range −2 (inactive) to +2 (active). [b] Molecular weight of the molecule, range 130.0–725.0. [c] Predicted octanol/gas partition coefficient, range 8.0–35.0. [d] Predicted water/gas partition coefficient, range 4.0–45.0. [e] Predicted octanol/water partition coefficient, range −2.0–6.5. [f] Predicted aqueous solubility, range −6.5–0.5. [g] Conformation-independent predicted aqueous solubility, range −6.5–0.5. [h] Predicted IC_{50} value for blockage of HERG K+ channels, range concern below −5. [I] Predicted apparent Caco-2 cell permeability in nm/sec. Caco-2 cells are a model for the gut-blood barrier, range <25 poor & >500 great. [j] Predicted brain/blood partition coefficient, range −3.0–1.2. [k] Number of likely metabolic reactions, 1–8. [l] Prediction of binding to human serum albumin, range −1.5–1.5. [m] Predicted human oral absorption on 0 to 100% scale, >80% is high & <25% is poor.

The number of sites of metabolism for compounds **5a**–**5e** have revealed that compounds in this series are metabolised through aryl nitro to NH_2, *para*-hydroxylation of aryl, and pyridine C2 hydroxylation. The metabolism of compound **6a**–**6e** series are metabolised through pyridine C2 hydroxylation, aryl nitro reduction to NH_2, ether dealkylation, and *para*-hydroxylation of aryl. We also checked whether our compounds in the series **5a**–**5e** and **6a**–**6e** are indeed new derivatives by performing a similarity search using QikProp v5.7 [34]. Compound **5a** shows a similarity index that spans from quinestradol 88.94, atovaquone 87.69, talniflumate 84.91, diphenpyramide 84.40, to quinestrol 84.00, respectively. Compound **5b** on the other hand shows a similarity index that spans from quinestradol 87.23, talniflumate 86.10, atovaquone 85.97, brovincamine 84.97, to ziprasidone 83.23. Compound **5c** is a new derivative because of its similarity index with quinestradol 89.24, atovaquone 88.15, mofezolac 85.26, diphenpyramide 84.84, and clometacin 83.96. Compound **5d** shows a similarity index with cilostazol 87.65,

vesnarinone 87.47, ketanserin 87.26, buspirone 84.39, and benperidol 84.15. Compound **5e** exhibits similarity index with cilostazol 88.50, quinestradol 86.17, benperidol 86.10, oxypertine 85.49, and timiperone 84.38.

Compound **6a** is a new derivative because it exhibits a similarity index with known compounds such as isofezolac 85.42, metaclazepam 83.70, oxetorone 82.73, quazepam 82.33, and thioridazine 82.32%. Compound **6b** is also a new derivative because it exhibited a similarity index with known compounds such as isofezolac 85.02, metaclazepam 84.94, quazepam 84.05, thioridazine 82.99, and pentagestrone 81.58%. Compound **6c** shows a similarity index that spans from isofezolac 84.08, oxetorone 84.07, midazolam 83.38, metaclazepam 83.11, and clemizole 82.67. Compound **6d** exhibits a similarity index that spans from isofezolac 85.42, metaclazepam 83.70, oxetorone 82.73, quazepam 82.33, and thioridazine 82.32% when compared with known compounds. Compound **6e** has a similarity index of quinestradol 86.42, clemizole 84.59, etoricoxib 83.89, talniflumate 83.73, and atovaquone 83.64%. Therefore, the compounds in this series **5a**–**5e** and **6a**–**6e** are newly synthesised derivatives which exhibit drug like properties because of their similarity indexes to known compounds ranging from 80–86%.

3. Materials and Methods

3.1. *General*

Chemical reagents were purchased from Sigma-Aldrich or Merck (Johannesburg, South Africa) and used without further purification. Melting points were obtained using Lasec/SA-melting point apparatus from Lasec Company, SA (Johannesburg, South Africa). IR spectra were recorded using a Agilent Technologies Cary 600 Series FT-IR spectrometer (Agilent

Technologies Australia [M] Pty Ltd., Mulgrave, Australia). NMR spectra were obtained using a Bruker Ascend 400 MHz NMR spectrometer (Bruker Biospin GmhH, Karlsrushe, Germany) operating at 400 MHz (^{1}H) and 100 MHz (^{13}C), where chemical shifts were quoted relative to the TMS peak. High-resolution mass spectra were recorded at an ionisation potential of 70 eV using a Waters Synapt G2 Quadrupole Time-of-flight mass spectrometer (Waters Corp., Milford, MA, USA) at the University of Stellenbosch Central Analytical Facility).

3.2. *Synthesis of 2-Aryl-quinazoline-4-one Derivatives* **3a**–**3e**

Quinazolinone derivatives **3a**–**3e** were prepared following a literature method [18]. To a 100 mL round bottom flask, anthranilamide **1a** (1 mmol), benzaldehyde derivatives **2a**–**2e** (1 mmol) and iodine (2 equiv.) in ethanol (30 mL per mmol of 1**a**) was refluxed at 80 °C for 6 h. The mixture was left to cool to room temperature and quenched with cold saturated sodium metabisulfate solution. The resulting precipitate was filtered and washed thoroughly with water. The solid product was recrystalised from acetonitrile and oven dried to yield the corresponding quinazoline-4(3*H*)-ones **3a**–**3e** [13]. The following products were prepared accordingly:

2-(4-Chlorophenyl)quinazolin-4(3H)-one (**3a**): A mixture of **1a** (1.50 g, 11.02 mmol), benzaldehyde (**2a**) (1.55 g, 11.02 mmol) and iodine (2.80 g, 22.04 mmol) in ethanol (100 mL) yielded 3a as a white solid (2.45 g, 87%); m.p. 295.2–297.1 °C, lit (298–299 °C) [13]; FT-IR(ν_{max}) 764, 840, 1168, 1232, 1259, 1531, 1606, 1666, 3052, 3174 cm^{-1}; ^{1}H-NMR (400 MHz, DMSO-d_6, ppm) 7.60–7.53 (m, 1H), 7.73–7.77 (m, 3H), 7.89–7.84 (m, 1H), 8.12–8.19 (m, 3H), 12.63 (s, 1H); ^{13}C-NMR (100 MHz, DMSO-d_6, ppm) 121.0, 125.2, 125.9, 126.8, 127.4, 129.8, 131.6, 131.9, 134.6, 148.5, 151.5, 162.2.

2-(4-Bromophenyl)quinazolin-4(3H)-one (**3b**): A mixture of **1a** (1.50 g, 11.02 mmol), benzaldehyde (2b) (2.00 g, 11.02 mmol) and iodine (2.80 g, 22.04 mmol) in ethanol (100 mL) yielded 3b as a white solid (3.01 g, 91%); m.p. >350 °C, lit (>350 °C) [13]; FT-IR(v_{max}) 766, 840, 1232, 1369, 1486, 1610, 1544, 1656, 3064, 3186 cm^{-1}; ^{1}H-NMR (400 MHz, DMSO-d_6, ppm) 7.68–7.54 (m, 1H), 7.63 (d, J = 8.4 Hz, 2H), 7.74 (d, J = 8 Hz, 1H), 7.95–7.86 (m, 1H), 8.15 (d, J = 8 Hz, 1H), 8.20 (d, J = 8.4 Hz, 2H) 12.63 (s, 1H); ^{13}C-NMR (100 MHz, DMSO-d_6, ppm) 121.0, 125.9, 126.8, 127.5, 128.7, 129.6, 131.6, 134.7, 136.3, 148.5 151.4, 162.2.

2-(4-Fluorophenyl)quinazolin-4(3H)-one (**3c**): A mixture of **1a** (1.50 g, 11.02 mmol), benzaldehyde (**2c**) (1.37 g, 11.02 mmol) and iodine (2.80 g, 22.04 mmol) in ethanol (100 mL) yielded 3c as a white solid (2.46 g, 93%); m.p. 261.3–263.2 °C, lit (257–259 °C) [13]; FT-IR(v_{max}) 764, 840, 1166, 1305, 1484, 1555, 1605, 1668, 3098, 3204 cm^{-1}; ^{1}H-NMR (400 MHz, DMSO-d_6, ppm) 7.24–7.35 (m, 3H), 7.71–7.77 (m, 2H), 8.09–8.15 (m, 3H), 12.58 (s, 1H) ; ^{13}C-NMR (100 MHz, DMSO-d_6, ppm) 115.4 (d, $^{2}J_{CF}$ = 22.2 Hz), 120.9, 125.9, 126.5, 128.9 (d, $^{4}J_{CF}$ = 2.9 Hz), 129.5, 130.1 (d, $^{3}J_{CF}$ = 9 Hz), 134.6, 148.7, 151.7, 163.8 (d, $^{1}J_{CF}$ = 249.2 Hz).

2-(4-Nitrophenyl)quinazolin-4(3H)-one (3d): A mixture of **1a** (1.50 g, 11.02 mmol), benzaldehyde (2d) (1.67 g, 11.02 mmol) and iodine (2.80 g, 22.04 mmol) in ethanol (100 mL) yielded 3d as a white solid (2.65 g, 90%); m.p. > 300 °C, lit (>300 °C) [13]; FT-IR(v_{max}) 741, 833, 1018, 1261, 1399, 1583, 1601, 1684, 3057, 3200; ^{1}H-NMR (400 MHz, DMSO-d_6, ppm) 7.38–7.68 (m, 1H), 7.72–7.51 (m, 2H), 8.21–8.42 (m, 5H), 12.882 (s, 1H) ; ^{13}C-NMR (100 MHz, DMSO-d_6, ppm) 121.4, 123.3, 123.6, 126.0, 126.8, 127.6, 129.0, 129.1, 134.3, 134.5, 139.9, 148.8, 152.1.

2-(4-Methoxyphenyl)quinazolin-4(3H)-one (**3e**): A mixture of **1a** (1.50 g, 11.02 mmol), benzaldehyde (2e) (1.50 g, 11.02 mmol) and iodine (2.80 g, 22.04 mmol) in ethanol (100 mL)

456 yielded 3e as a white solid (2.58 g, 93%); 242.7–243.4 °C, lit (240–241 °C) [13]; FT-IR(v_{max})
457 703, 888, 1086, 1380, 1477, 1566, 1691, 1699, 3011, 3247; ^{1}H-NMR (400 MHz, DMSO-d_6,
458 ppm) 3.84 (s, 3H), 7.08 (d, *J* = 14.8 Hz, 2H), 7.61–7.48 (m, 1H), 7.70 (d, *J* = 7.6 Hz, 1H),7.93–
459 7.80 (m, 1H), 8.19 (d, *J* = 14.8 Hz, 2H), 12.43 (s, 1H); ^{13}C-NMR (100 MHz, DMSO-d_6, ppm)
460 55.46, 114.0, 120.7, 124.9, 125.8, 126.1, 127.1, 129.5, 134.5, 148.9, 152, 161.9, 162.4.

461 3.3. *Oxidative aromatisation of* **3a**–**3e** *in* $SOCl_2$*-DMF mixture*

462 4-Chloroquinazoline derivatives were prepared following a literature method reported by
463 Mphahlele and co-workers [16]. To a stirring suspension of 3**a** (1.00 g, 3.90 mmol) in thionyl
464 chloride (30 mL) at room temperature, DMF (1 mL) was added dropwise. The mixture was
465 refluxed for 2 h and allowed to cool to room temperature before quenching with cold water and
466 was extracted with dichloromethane. The dichloromethane was dried over anhydrous sodium
467 sulphate, filtered and evaporated under reduced pressure to yield compounds **4a**–**4d** [14] and **4e**
468 [15]. The following products were prepared accordingly.

469 *4-Chloro-2-(4-chlorophenyl)quinazoline* (**4a**). A stirred mixture of **3a** (1.00 g, 3.90 mmol) and
470 DMF (1 mL) in thionyl chloride (30 mL) yielded 4a as a white solid (0.94 g, 88%); m.p. 143.2–
471 145.4 °C; FT-IR(v_{max}) 758, 842, 954, 1152, 1234, 1336, 1519, 1537; ^{1}H-NMR(400 MHz, $CDCl_3$,
472 ppm) 7.47 (d, *J* = 8.8 Hz, 2H), 7.60–7.56 (m, 1H), 7.89–7.85 (m, 1H), 8.05 (d, *J* = 8 Hz, 1H),
473 8.23 (d, *J* = 8 Hz, 1H), 8.56 (d, *J* = 8.8 Hz, 2H); ^{13}C-NMR (100 MHz, $CDCl_3$, ppm) 122.4, 125.8,
474 128.4, 128.9, 130.1, 135.0, 137.4, 143.7, 151.7, 159, 162.6. [14]

475 *2-(4-Bromophenyl)-4-chloroquinazoline* (**4b**). A stirred mixture of **3b** (1.00 g, 3.30 mmol) and
476 DMF (1 mL) in thionyl chloride (30 mL) yielded 4b as a white solid (1.13 g, 93%); m.p. 151.7–
477 153.4 °C; FT-IR(v_{max}) 647, 699, 742, 785, 844, 902, 1152, 1264, 1339, 1600; ^{1}H-NMR (400

MHz, $CDCl_3$, ppm) 7.48–7.54 (m, 3H) 7.94–7.90 (m, 1H), 8.05 (d, *J* = 8.4 Hz, 1H), 8.22 (d, *J* = 8.4 Hz, 1H), 8.43 (d, *J* = 8.8 Hz, 2H); ^{13}C-NMR(100 MHz, $CDCl_3$, ppm) 122.4, 125.8, 128.8, 130, 131.8, 135, 135.5, 137.3, 151.6, 159.0, 162.6. [14]

4-Chloro-2-(4-fluorophenyl)quinazoline (**4c**). A stirred mixture of **3c** (1.00 g, 4.18 mmol) and DMF (1 mL) in thionyl chloride (30 mL) yielded **4c** as a white solid (0.97 g, 90%); m.p. 137.2–139.3 °C; FT-IR(v_{max}) 655, 688, 726, 760, 844, 933, 1153, 1264, 1510, 1563; ^{1}H-NMR (400 MHz, $CDCl_3$, ppm) 7.11–7.28 (m, 2H), 7.66–7.62 (m, 1H), 7.94–7.89 (m, 1H), 8.05 (d, *J* = 8 Hz, 1H), 8.23 (d, *J* = 8 Hz, 1H), 8.41–8.46 (m, 2H); ^{13}C-NMR (100 MHz, $CDCl_3$, ppm) 115.7 (d, $^2J_{CF}$ = 24 Hz), 122.3, 128.2, 128.8, 130.9 (d, $^3J_{CF}$ = 8.8 Hz), 132.9 (d, $^4J_{CF}$ = 3 Hz), 151.8, 159, 162.5, 165.1 (d, $^1J_{CF}$ = 248.5 Hz). [14]

4-Chloro-2-(4-nitrophenyl)quinazoline (**4d**). A stirred mixture of **3d** (1.00 g, 3.74 mmol), v_{max} (ATR) and DMF (1 mL) in thionyl chloride (30 mL) yielded 4d as a white solid (0.90 g, 84%); m.p. 148.1–150.2 °C; FT-IR(v_{max}) 709, 843, 891, 1026, 1248, 1322, 1373, 1509, 1587; ^{1}H-NMR (100 MHz, $CDCl_3$, ppm) 7.76–7.72 (m, 1H), 8.01–7.97 (m, 1H), 8.13 (d, *J* = 8.4 Hz, 1H), 8.29 (d, *J* = 8.4 Hz, 1H), 8.34 (d, *J* = 10.4 Hz, 2H), 8.74 (d, *J* = 10.4 Hz, 2H); ^{13}C-NMR (400 MHz, $CDCl_3$, ppm) 122.7, 123.7, 125.9, 129.5, 129.6, 135.3, 142.3, 144.2, 149.4, 151.6, 157.7, 162.9. [14]

4-Chloro-2-(4-methoxyphenyl)quinazoline (**4e**). A stirred mixture of **3e** (1.00 g, 3.98 mmol) and DMF (1 mL) in thionyl chloride (30 mL) yielded **4e** as a white solid (0.96, 89%); m.p. 144.3–146.6 °C; FT-IR(v_{max}) 763, 837, 934, 1152, 1290, 1336, 1579, 1603; ^{1}H-NMR (400 MHz, $CDCl_3$, ppm) 3.87 (3H, br-s), 7.08 (d, *J* = 8.8 Hz, 2H), 7.97–7.93 (m, 1H), 7.67–7.63 (m, 1H), 8.01 (d, *J* = 8 Hz, 1H), 8.17 (d, *J* = 8 Hz, 1H), 8.52 (d, *J* = 8.8 Hz, 2H); ^{13}C-NMR (100 MHz,

500 $CDCl_3$, ppm) 55.4, 113.9, 122.0, 125.8, 127.7, 128.5, 129.2, 130.4, 134.7, 151.8, 159.8, 162.1,
501 162.2. [15]

502 3.4. *Typical Procedure for Dechloroamination of* **4a**–**4e**

503 A stirred mixture of **4a** (1 equiv.), 2-amino-3-nitropyridine 1.1 equiv.) and concentrated
504 sulfuric acid (20 drops) in (3:1) THF-DMF 30 mL was heated at 65 °C for 5 h after which the
505 solution was allowed to cool to RT. The reaction mixture was then added to crushed ice, stirred
506 and the product extracted with ethyl acetate. The organic layer was washed with aqueous
507 solution of sodium hydrogen carbonate, dried over anhydrous sodium sulfate, filtered and
508 evaporated under reduced pressure to afford **5a**–**5e** as yellow solids. The following compounds
509 were prepared accordingly:

510 *2-(4-Chlorophenyl)-N-(3-nitropyridin-2-yl)quinazolin-4-amine* (**5a**). A mixture of 4-chloro-
511 2-(4-chloro-phenyl)quinazoline (**4a**, 0.30 g, 1.09 mmol), sulphuric acid 20-drops and 2-amino-3-
512 nitropyridine (0.17 g, 1.20 mmol) in THF-DMF, 30 mL (3:1) afforded **5a** as yellow solid (0.28 g,
513 95%) m.p. 281.2–282.1 °C; FT-IR (v_{max}) 458, 478, 538, 683, 728, 761, 840, 1012, 1074, 1149,
514 1241, 1280, 1344, 1344, 1443, 1556, 1599, 1669, 3132, 3461; ^{1}H-NMR (400 MHz, DMSO-d_6,
515 ppm) 6.73–6.76 (dd, J = 4.8 Hz and 4.4 Hz, 1H), 7.56–7.52 (m, 1H), 7.63 (d, J = 8.8 Hz, 2H),
516 7.75 (d, 8.0 Hz, 1H), 7.87–7.84 (m, 1H), 7.90 (s, 1H), 8.16 (d, J = 8.0 Hz, 1H), 8.20 (d, J = 8.8
517 Hz, 2H), 4.00–8.34 (m, 1H), 12.63 (s, 1H); ^{13}C-NMR (100 MHz, DMSO-d_6, ppm) 113.0, 121.5,
518 126.4, 127.3, 128, 129.2, 130.1, 132, 135.2, 135.4, 136.8, 149, 151.8, 154.2, 156.8, 162.6; *m*/*z*
519 calculated 377.0680, HRMS(ESI): $[M\text{-}HCl]^+$, $C_{19}H_{11}N_5O_2^+$, found 340.9927.

520 *2-(4-Bromophenyl)-N-(3-nitropyridin-2-yl)quinazolin-4-amine* (**5b**). A mixture of 2-(4-
521 bromophenyl)-4-chloroquinazoline (**4b**, 0.30 g, 0.94 mmol), sulphuric acid 20-drops and 2-

amino-3-nitropyridine (0.14 g, 1.03 mmol) in THF-DMF, 30 mL (3:1) afforded **5b** as yellow solid (0.21 g, 78%), m.p. 292.1–284.1 °C; FT-IR(v_{max}) 389, 505, 545, 771, 799, 1008, 1064, 1150, 1182, 1336, 1480, 1558, 1600, 1670, 2884, 2919, 2960, 3027, 3268, 3462; ^{1}H-NMR (400 MHz, DMSO-d_6, ppm); 6.73–6.76 (dd, J = 4.63 Hz and J = 4.44 Hz, 1H), 7.56–7.51 (m, 1H), 7.73–7.78 (m, 3H), 7.86–7.82 (m, 1H), 7.72 (s, 1H), 8.10–8.16 (m, 3H), 8.19–8.40 (m, 1H), 12.64 (s, 1H); ^{13}C-NMR (100 MHz, DMSO-d_6, ppm) 112.5, 121.0, 125.3, 125.7, 126.8, 126.8, 127.5, 129.9, 131.7, 132.0, 135.0, 148.6, 151.5, 153.8, 156.3, 162.3; *m*/*z* calculated 421.0174, HRMS (ESI): $[M+Na]^+$, $C_{19}H_{12}{}^{79}BrN_5O_2Na^+$, found 444.9536.

2-(4-Fluorophenyl)-N-(3-nitropyridin-2-yl)quinazolin-4-amine (**5c**). A mixture of 4-chloro-2-(4-fluorophenyl)quinazoline (**4c**, 0.30 g, 1.16 mmol), sulphuric acid 20-drops and 2-amino-3-nitropyridine (0.18 g, 1.28 mmol) in THF-DMF, 30 mL (3:1) afforded **5c** as yellow solid (0.26 g, 92%),m.p. 273.8–274.8 °C; FT-IR(v_{max}) 426, 496, 540, 685, 735, 763,802, 840, 940, 1019, 1110, 1149, 1233, 1321, 1446, 1518, 1580, 1667, 3090, 3463; ^{1}H-NMR (400 MHz, DMSO-d_6, ppm) 6.73–6.76 (dd, J = 4.4 Hz and 4.4 Hz, 1H), 7.41–7.37 (m, 2H), 7.54–7.50 (m, 1H), 7.74 (d, J = 8 Hz, 1H), 7.84 (t, J = 15.6 Hz, 1H), 7.89 (1H, s), 8.15 (d, J = 7.6 Hz, 1H), 8.14–8.23 (m, 2H), 8.39–8.36 (m, 1H), 12.58 (s, 1H); ^{13}C-NMR (100 MHz, DMSO-d_6, ppm) 113.0, 115.7 (d, $^{2}J_{CF}$ = 21.8 Hz), 121.3, 126.3, 127.1, 127.2, 127.9, 129.3 (d, $^{4}J_{CF}$ = 2.9 Hz), 130.4 (d, $^{3}J_{CF}$ = 9.2 Hz), 135.1, 135.4, 149.1, 151.9, 154.2, 156.7, 164.2 (d, $^{1}J_{CF}$ = 249.4 Hz); *m*/*z* calculated 361.0975 , HRMS (ESI): $[M]^+$, $C_{19}H_{12}FN_5O_2{}^+$, found 361.0641.

2-(4-Nitrophenyl)-N-(3-nitropyridin-2-yl)quinazolin-4-amine (**5d**). A mixture of 4-chloro-2-(4-nitrophenyl)quinazoline (**4d**, 0.30 g, 1.05 mmol), sulphuric acid 20-drops and 2-amino-3-nitropyridine (0.16 g, 1.16 mmol) in THF-DMF, 30 mL (3:1) afforded **5d** as yellow solid (0.18 g, 66%), m.p. 269.2–271.2 °C; FT-IR(v_{max}) 501, 539, 762, 802, 820, 941, 1030, 1070, 1099, 1149,

1175, 1241, 1440, 1410, 1515, 1561, 1598, 1674, 3133, 3462; ^{1}H-NMR (400 MHz, DMSO-d_6, ppm); 6.73–6.76 (dd, J = 4.53 Hz and J = 4.59 Hz, 1H), 7.58–7.54 (m, 1H), 7.79 (d, J = 7.63 Hz, 1H), 7.88–7.84 (m, 1H), 7.93 (s, 1H), 8.18 (d, J = 7.63 Hz, 1H), 7.86–8.44 (m, 6H), 12.89 (s, 1H); ^{13}C-NMR (100 MHz, DMSO-d_6, ppm) 112.5, 121.3, 123.7, 126.0, 127.8, 127.7, 129.3, 135, 139.1, 148.5, 148.9, 151.3, 153.8, 156.3, 162.7; *m*/*z* calculated 388.0920, HRMS (ESI): $[M+Na]^+$, $C_{19}H_{12}N_6O_4Na^+$, found 411.0530.

2-(4-Methoxyphenyl)-N-(3-nitropyridin-2-yl)quinazolin-4-amine (**5e**). A mixture of 4-chloro-2-(4-methoxyphenyl)quinazoline (4e, 0.30 g, 1.11 mmol), sulphuric acid 20-drops and 2-amino-3-nitropyridine (0.17 g, 1.22 mmol) in THF-DMF, 30 mL (3:1) afforded 5e as yellow solid (0.24 g, 84%), m.p. 262.4–264.4 °C; FT-IR(v_{max}) 423, 504, 540, 575, 611, 762, 835, 940, 1119, 1244, 1291, 1415, 1441, 1483, 1517, 1558, 1599, 1668, 2994, 3464; ^{1}H-NMR(400 MHz, DMSO-d_6) 3.85 (s, 3H), 6.73–6.76 (dd, J = 4.67 Hz and J = 4.47 Hz, 1H), 7.09 (d, J = 9.14 Hz, 2H), 7.50–7.46 (m, 1H), 7.70 (d, J = 8.36 Hz, 1H), 7.84–7.79 (m, 1H), 7.91 (s, 1H), 8.13 (d, J = 8.36 Hz, 1H), 8.19 (d, J = 9.14 Hz, 2H), 8.20–8.40 (m, 1H), 12.43 (s, 1H); ^{13}C-NMR(100 MHz, DMSO-d_6) 55.5, 112.5, 114.0, 120.7, 124.8, 125.9, 126.2, 126.8, 127.3, 129.5, 134.6, 135, 149.0, 151.9, 153.8, 156.3, 161.9, 162.4; *m*/*z* calculated 373.1175, HRMS(ESI): $[M]^+$, $C_{20}H_{15}N_5O_4^+$, found 373.1553.

3.5. *Typical Procedure for Sonogashira Cross-Coupling of* **4a**–**4e** *with 4-Ethynylpyridine*

A mixture of 4 (1 equiv.), $PdCl_2(PPh_3)_2$ (10%), CuI (10%) and Cs_2CO_3 (2 equiv.) in 3:1 THF-water, in a round-bottom flask equipped with a stirrer bar and a condenser equipped with a balloon was flushed for 5 min with nitrogen gas. 1.5 equiv. 4-thynylpyridine hydrochloride was added to the flask at once and the mixture was flushed for an additional 10 min. The mixture was refluxed for 24 h at 65 °C under nitrogen atmosphere and then quenched with ice cold water. The

precipitate was filtered on a sintered funnel and then taken up into dichloromethane. The solution was dried with sodium sulfate, filtered and then evaporated under reduced pressure. The residue was recrystallised from diethyl ether to afford 4-(ethynylpyridine)quinazolines **6a**–**6e**.

2-(4-Chlorophenyl)-4-(2-(pyridin-4-yl)ethynyl)quinazoline (**6a**), A mixture of 4-chloro-2-(4-chlorophenyl)quinazoline **(4a**, 0.50 g, 1.82 mmol), $PdCl_2(PPh_3)_2$ (0.13 g, 0.18 mmol), CuI (0.04 g, 0.18 mmol), Cs_2CO_3 (1.19 g, 3.64 mmol) and 4-ethynylpyridine hydrochloride (0.38 g, 2.73 mmol) in THF-water, 30 mL (3:1) afforded **6a** as white solid (0.46 g, 98%); m.p. 209.2–210.0 °C; FT-IR(v_{max}) 759, 845. 881, 1024, 1228, 1252, 1433, 1537, 2221; ^{1}H-NMR (400 MHz, $CDCl_3$, ppm) 7.50 (d, *J* = 8.4 Hz, 2H), 7.61 (d, *J* = 5.2 Hz, 2H), 7.70–7.67 (m, 1H), 7.97–7.93 (m, 1H), 8.10 (d, *J* = 8.4 Hz, 1H), 8.33 (d, *J* = 8.4 Hz, 1H), 8.59 (d, *J* = 8.4 Hz, 2H), 8.74 (d, *J* = 5.2 Hz, 2H); ^{13}C-NMR (100 MHz, $CDCl_3$, ppm) 88.8, 93.7, 123.8, 125.9, 126.1, 128.2, 128.9, 129.2, 129.4, 130.1, 134.7, 136.0, 137.1, 150.1, 151.1, 151.9, 159.9; *m*/*z* calculated 341.0720, HRMS(ESI): $[MH]^+$, $C_{21}H_{12}{}^{35}ClN_3{}^+$, found 342.0787.

2-(4-Bromoyphenyl)-4-(2-(pyridin-4-yl)ethynyl)quinazoline (**6b**), A mixture of 2-(4-bromophenyl)-4-chloroquinazoline (**4b**, 0.50 g, 1.56 mmol), $PdCl_2(PPh_3)_2$ (0.11 g, 0.17 mmol), CuI (0.03 g, 0.16 mmol), Cs_2CO_3 (1.02 g, 3.12 mmol) and 4-ethynylpyridine hydrochloride (0.33 g, 2.35 mmol) in THF-water, 30 mL (3:1) afforded **6b** white solid (0.40 g, 90%); m.p. 234.6–236.3 °C ; FT-IR(v_{max}) 767, 1005, 1023, 1264, 1336, 1532, 2225; ^{1}H-NMR (400 MHz, $CDCl_3$, ppm) 7.60 (d, *J* = 6 Hz, 2H), 7.64–7.70 (m, 3H), 7.96–7.92 (m, 1H), 8.10 (d, *J* = 8.4 Hz, 1H), 8.33 (d, *J* = 8.4 Hz, 1H), 8.68 (d, *J* = 13.2 Hz, 2H), 8.74 (d, *J* = 6 Hz, 2H); ^{13}C-NMR (100 MHz, $CDCl_3$, ppm) 89.0, 93.7, 123.8, 125.7, 125.9, 126.1, 128.2, 129.1, 129.3, 130.2, 131.8, 134.7, 136.4, 150.1, 151.0, 151.9, 159.9; *m*/*z* calculated 386.0215, HRMS(ESI): $[MH^+]$, $C_{19}H_{12}{}^{81}BrN_3{}^+$, found 388.0274.

2-(4-Fluorophenyl)-4-(2-(pyridin-4-yl)ethynyl)quinazoline (**6c**), A mixture of 4-chloro-2-(4-fluorophenyl)quinazoline (**4c**, 0.50 g, 1.93 mmol), $PdCl_2(PPh_3)_2$ (0.14 g, 0.19 mmol), CuI (0.04 g, 0.19 mmol), Cs_2CO_3 (1.23 g, 3.86 mmol) and 4-ethynylpyridine hydrochloride (0.40 g, 2.90 mmol) in THF-water, 30 mL (3:1) afforded **6c** as a white solid (0.39 g, 94%); m.p. 197.6–199.2 °C; FT-IR(ν_{max}) 758, 819, 925, 1147, 1270, 1336, 1537, 2220; ^{1}H-NMR (400 MHz, $CDCl_3$, ppm) 7.23–7.19 (m, 2H), 7.60 (d, *J* = 6 Hz, 2H), 7.70–7.66 (m, 1H), 7.96–7.92 (m, 1H), 8.09 (d, *J* = 8.4 Hz, 1H), 8.32 (d, *J* = 8.4 Hz, 1H), 8.41–8.67 (m, 2H), 8.73 (d, *J* = 6 Hz, 2H); ^{13}C-NMR (100 MHz, $CDCl_3$, ppm) 88.9, 93.6, 115.6 (d, $^2J_{CF}$ = 21.5 Hz), 123.7, 126, 128, 129.1, 129.4, 130.8 (d, $^3J_{CF}$ = 8.7 Hz), 133.7 (d, $^4J_{CF}$ = 2.9 Hz), 134.7, 150.2, 151.5, 160.1, 164.7 (d, $^1J_{CF}$ = 247.6 Hz); *m*/*z* calculated 325.1015, HRMS(ESI): $[MH]^+$, $C_{21}H_{12}FN_3^+$, found 326.1082.

2-(4-Nitrophenyl)-4-(2-(pyridin-4-yl)ethynyl)quinazoline (**6d**), A mixture of 4-chloro-2-(4-nitrophenyl)quinazoline (**4d**, 0.50 g, 1.75 mmol), $PdCl_2(PPh_3)_2$ (0.12 g, 0.18 mmol), CuI (0.33 g, 0.18 mmol), Cs_2CO_3 (1.14 g, 3.50 mmol) and 4-ethynylpyridine hydrochloride (0.37 g, 2.63 mmol) in THF-water, 30 mL (3:1) afforded **6d** as a white solid (0.39 g, 94%); m.p. 272.7–274.8 °C; FT-IR(ν_{max}) 714, 819, 930, 1215, 1250, 13338, 1592, 2207; ^{1}H-NMR (400 MHz, $CDCl_3$, ppm) 7.61 (d, *J* = 5.60 Hz, 2H), 7.71–7.74 (m, 1H), 8.03–7.98 (m, 1H), 8.16 (d, *J* = 8.77 Hz, 1H), 8.16–8.35 (m, 3H), 8.75 (d, *J* = 5.01 Hz, 2H), 8.83 (d, *J* = 9.19 Hz, 2H); ^{13}C-NMR (100 MHz, $CDCl_3$, ppm) 88.4, 94.1, 123.6, 123.9, 125.8, 126.0, 128.3, 128.4, 128.4, 129.1, 129.2, 129.3, 134.9, 143.1, 149.1, 149.8, 150.1, 150.8, 151.9, 158.4; *m*/*z* calculated 352.1015, HRMS(ESI): $[MH]^+$, $C_{21}H_{12}N_4O_4^+$, found 353.1027.

2-(4-Methoxyphenyl)-4-(2-(pyridin-4-yl)ethynyl)quinazoline (**6e**), A mixture of 4-chloro-2-(4-nitrophenyl)quinazoline (**4d**, 0.50 g, 1.85 mmol), $PdCl_2(PPh_3)_2$ (0.13 g, 0.19 mmol), CuI (0.04 g, 0.19 mmol), Cs_2CO_3 (1.21 g, 3.70 mmol) and 4-ethynylpyridine hydrochloride (0.39 g, 2.78

614 mmol) in THF-water, 30 mL (3:1) afforded **6e** as a yellow solid (0.50 g, 79%) ; m.p. 202.6–
615 204.6 °C; FT-IR(v_{max}) 761, 818, 924, 1161, 1252, 1360, 1468, 1535, 2219; ^{1}H-NMR (400 MHz,
616 $CDCl_3$, ppm); 3.88 (s, 3H), 7.03 (d, *J* = 8.87 Hz, 2H), 7.58–7.62 (m, 15.97 Hz, 3H), 7.90–7.86
617 (m, 1H), 8.05 (d, *J* = 8.87 Hz, 1H), 8.27 (d, *J* = 8.87 Hz, 1H), 8.57 (d, *J* = 8.87 Hz, 2H), 8.72 (d,
618 *J* = 3.52 Hz, 2H); ^{13}C-NMR (100 MHz, $CDCl_3$, ppm) 55.4, 89.0, 93.2, 113.9, 123.4, 125.9, 126,
619 127.4, 129.5, 130.1, 130.3, 134.4, 150.1, 151.1, 151.6, 160.6, 161.9; *m/z* calculated 337.0215,
620 HRMS(ESI): $[MH]^+$, $C_{22}H_{15}N_3O^+$, found 338.1286.

621 3.6. *Mycobacterium tuberculosis H_{37}Rv Minimum Inhibitory Concentration (MIC_{90}) Assay*

622 The inhibitory activity against *Mycobacterium tuberculosis* was achieved at the University
623 of Cape Town, Drug Discovery and Development Centre (H3-D), following the broth
624 microdilution method. The broth microdilution method allows a range of antibiotic
625 concentrations to be tested on a single 96-well microtitre plate in order to determine the
626 minimum inhibitory concentration (MIC). Briefly, a 10 mL culture of a mutant *Mtb* (H_{37}Rv)
627 strain constitutively expressing recombinant alamar blue assay of a plasmid integrated at the attB
628 locus is grown to an OD600 of 0.6–0.7. The Mtb. H_{37}Rv strain culture is then diluted 1:100 in
629 7H9 GLU CAS TX. In a 96-well microtitre plate, 50 µL of 7H9 GLU CAS TX medium is added
630 to all wells from Rows 2–12. The compounds to be tested are added to Row 2–12 in duplicates,
631 at a final concentration of 640 µM (stocks are made up to a concentration of 12.8 mM in DMSO,
632 and diluted to 640 µM in 7H9 GLU CAS TX medium). A two-fold serial dilution is prepared, by
633 transferring 50 µL of the liquid in Row 1 and 2 to mix. 50 µL of the liquid in Row 2 was then
634 transferred to Row 3 and aspirated. The procedure was repeated until Row 12 is reached, from
635 which 50 µL of the liquid is discarded to bring the final volume in all wells to 50 µL. Finally, 50
636 µL of the 1:100 diluted Mtb cultures are added to all wells in Rows 2–12. Row 1 serves as a

637 contamination control which includes media, 5% DMSO and rifampicin. The microtitre plate is
638 stored in a secondary container and incubated at 37 °C with humidifier to prevent evaporation of
639 the liquid. The lowest concentration of compounds which inhibit growth of more than 90% of the
640 bacterial population was considered to be the MIC_{90}. The pellet data is reported as visual score
641 and calculated MIC during 7 and 14 day post inoculation [35].

642 3.7. *MTT Cell Viability Assay Protocol*

643 MTT assay was carried out to determine the growth inhibitory effects of compounds **6a**–**6e**
644 on Raw 264.7 microphage cell line at a maximum concentration of 50 µM. Cells were seeded at
645 a density of 1×10^4 cells/well and then cultured in a humidified incubator at 37 °C overnight.
646 After overnight incubation, cells were treated with 0.1% dimethyl sulfoxide (DMSO), 50 µM
647 curcumin (positive control) and various concentrations of the compounds for 24 hours. The wells
648 which contained only the media served as untreated control. After 24 hours treatment, 10 µL of
649 MTT (5 mg/mL) was added to each well and incubated for 4 hours at 37 °C. The MTT
650 containing medium was carefully removed after 4 hours of incubation to prevent disruption of
651 the crystals at the bottom of the wells and 100 µL of DMSO was added to solubilize the purple
652 formazan crystals. The optical density was measured using Glomax-Multi microplate reader
653 (Promega, Madison, WI, USA) at 560 nm. The relative cell viability was expressed as [(Abs
654 $_{sample}$/Abs $_{control}$) × 100%].

655 3.8. *Methodology for Molecular Docking*

656 3.8.1. Software Program

657 Maestro (v11.5) [36], a graphical user interface (GUI) for the Schrödinger Suite 2015, was
658 used to perform all simulation tasks. The GUI has built-in work-flows of all Schrödinger

659 modules in the life-sciences suite. The software license is freely available at the Centre for High
660 Performance Computing (CHPC) Linux cluster, available to all academic users in South Africa.

661 3.8.2. Protein Preparation

662 The Protein Data Bank (PDB) was searched to locate the X-ray crystal structure of a relaxed
663 Glutamine Synthetase from *Mycobacterium tuberculosis*, PDB ID: 1HTO, 3ZXR, and 3ZXV.
664 1HTO structure is co-crystalized with native ligand Adenosine monophosphate with a resolution
665 of 2.4 Å [37]. On the other hand, 3ZXR is complexed with compound **3** and 3ZXV is complexed
666 with compound **2** at a resolution of 2.15 and 2.26 Å, respectively Gising et al [11]. Firstly, the
667 pdb structures were imported into Maestro [36] and the structure of the enzyme was prepared by
668 using the Protein Preparation Wizard [38,39]. The PDB structure in the workspace was pre-
669 processed using default parameters in order to assign bond orders, create zero bonds to metals,
670 create disulfide bonds, fill in missing chains and loops using Prime automatically [40–42]. The
671 protonation states of the protein and co-crystalized ligand were sampled by using Epik [43–45] at
672 pH 7.4. Since the PDB structures are multimers all chains were deleted leaving only chain A and
673 B. Hydrogen bond assignment was optimized to sample water orientations, through the use of
674 crystal symmetry and minimizing hydrogens of altered species. Interactive optimizer was
675 performed at pH 7.0 using PROPKA [46] in order to reduce steric clashes. Waters within 3Å of
676 the heteroatoms in the active site were removed. Restrained minimization was performed with
677 OPLS_2005 force field [47,48] to attain convergence to RMSD 0.30 Å. The protein grid was
678 prepared by marking the active site using the co-crystallized ligand structures. Hydrogen bond
679 constraints were marked by the amino acids that form hydrogen bonds with the ligand. The metal
680 coordination constraints were enforced by marking the metal coordination between the ligand
681 and metals.

682 3.8.3. Ligand Preparation

683 The ligands were drawn by virtue of using Maestro's [36] 2D sketcher. The resulting 2D
684 structures were imported into Maestro [36] as 3D coordinates. The structures were imported into
685 LigPrep [49], a module built-in into Maestro. The tautomeric and/or ionization states for each of
686 the ligands were made by Epik [43–45] at pH 7.4 to mimic physiological conditions.
687 OPLS_2005 force-field [47,48] was used to generate conformers of the compounds.
688 Stereoisomers were computed by retaining specified chiralities.

689 3.8.4. Glide XP Docking

690 The prepared structures from Section 3.8.3 were imported as input structures for Glide XP
691 docking [50–53] protocol. The prepared and minimized structure of the grid of the enzymes from
692 Section 3.8.2 was selected. The extra precision (XP) protocol for docking was selected to
693 generate up to 20 poses. Conformational changes during docking were measured by using
694 OPLS_2005 force-field [47,48]. Conformational sampling was accounted for by using default
695 parameters and sampling only ring conformations. Docking was undertaken by using Glide [54–
696 57], in the extra precision mode using rigid body docking [51]. The final docking run occurs
697 when the best docking poses as outputs were ranked by using the XP Glide score [51].

698 3.9. *Single Crystal Ctructure Determination.*

699 Crystal evaluation and data collection was done on a Bruker Smart APEXII diffractometer
700 with Mo Ka radiation (I = 0.71073 Å) equipped with an Oxford Cryostream low temperature
701 apparatus operating at 100 K for all samples. Reflections were collected at different starting
702 angles and the *APEX*II program suite was used to index the reflections [58]. Data reduction was
703 performed using the *SAINT* [59] software and the scaling and absorption corrections were

applied using the *SADABS* [60] multi-scan technique. The structures were solved by the direct method using the *SHELXS* program and refined using *SHELXL* program [61]. Graphics of the crystal structures were drawn using Mercury software [62]. Non-hydrogen atoms were first refined isotropically and then by anisotropic refinement with the full-matrix least square method based on F^2 using *SHELXL*. Data-Deposition Number 1953828.

4. Conclusions

The 4-pyridylquinazoline derivatives **5a**–**5e** and **6a**–**6e** were successfully synthesised using literature methods detailing dechloroamination and Sonogashira cross-coupling of the requisite 4-chloroquinazolines **4a**–**4e**. Structure activity relationship (SAR) investigations on the *C(4)* position of compounds **4a**–**4e** yielded moderate to good MIC_{90} activity for compounds **5b** and **5e** for the 4-pyridylamino series and also for **6a**, **6b**, **6d** and **6e** for the 4-ethynylpyridine series when assayed against $H_{37}Rv$ strain of *Mtb*. Notable MIC_{90} potency was observed for **6a**, **6b** and **6e** at 9.82 µM, 9.39 µM and <0.72 µM respectively when compared to rifampicin. These compounds *i.e,* **6a, 6b** and **6e** were also found to possess low toxicity against Raw 267.4 microphages with IC_{50} values >50 µM. The selectivity indexes (SI) calculated were >10 for compounds **6b** and **6e**. Based on this in vitro data, compound **6e** was identified as a key candidate which showed good antimycobacterial activity. Cross-docking docking was able to assist in establishing the most accurate crystal structure of glutamine synthetase amongst three PDB structures i.e. 1HTO, 3ZXR, and 3ZXV. The cross-docking studies revealed that the binding mode of compound **3** co-crystallized onto 3ZXR was reproduced with an RMSD of 0.28 Å. Further docking of compound **2** and AMP using classical Glide XP, reproduced the native binding mode when docking into 3ZXR. While their native pdb structures did not reproduce their native bound conformations. Therefore, 3ZXR was then used for further studies for compounds

in the **5a**–**5e** and **6a**–**6e** series, into the active site cavity of glutamine synthetase (PDB:3ZXR). Classical Glide XP docking revealed that compounds in the **6** series follows the same binding mode as compound **2** and **3** from Gising et al. This is because of the hydrogen bond between the OH group of SER280 and Nitrogen of pyridine ring of compounds in the **6** series as well as metal coordination with Mg^{2+} (see Fig. 5a, b and c). On the other hand, compounds in the **5** series have exhibited a different binding mode. Since, they prefer binding below the Mg^{2+} ion moiety. Even though, SER280 hydrogen bonds with the nitro group of nitropyridine ring moiety of compounds in the **5** series (see Fig. 5d). The physicochemical ADME properties confirmed compounds from both series **5a**–**5e** and **6a**–**6e** exhibiting drug like properties since they share at least 86% (on average) similarity with the generated commercial drugs. Given the synergy between the structure activity relationships in silico with both MIC_{90} and IC_{50} for the nitrobenzene (**5a**–**5e**) and nitropyridine (**6a**–**6e**) compounds, further derivatization of these ligands could be useful for optimization or design.

Author statement:

Author Contributions: The experimental component and NMR data interpretation was conducted by K.B.D. and N.R.M. under direct supervision of the lead author R.M.M. who has conceptualized and designed the project, W.N. provided assistance with mass spectra data interpretation and reviewed the manuscript while T.M.M. and D.M performed bio assays and their respective interpretations, N.G. performed all computational experiments and their respective interpretation while B.O. assisted with crystal structure determination and interpretation. All authors have read and approved the final manuscript.

Conflicts of Interest: The authors declare no conflict of interest.

Funding: The authors are grateful for financial support on this project from the University of Limpopo (UL) and the National Research Foundation (South Africa) through grant number TTK150612119362 and the Sasol Inzalo Foundation for financial support.

Acknowledgements: The authors wish to thank Prof M.J. Mphahlele (University of South Africa) for his continuous support and intellectual discussions, University of Stellenbosch Central Analytical Facility (CAF) and the Drug Discovery and Development Centre (H3D) at the University of Cape Town for mass spectrometric and *Mtb* assay data, respectively. The authors also wish to acknowledge the Centre for High Performance (CHPC) in Cape Town for the access to their High Performance Computing cluster and also access to the software license.

Supplementary Materials:

References

1. N. Fogel, Tuberculosis: A disease without boundaries. Tuberculosis 95 (2015) 527–531.
2. World Health Organization. *Global Tuberculosis Report*; CC BY-NC-SA 3.0 IGO; Licence: Geneva, Switzerland, 2018.
3. E. Jafara, M.R Khajouei, F. Hassanzadeh, G.H Hakimelahi, G.A Khodarahmi, Quinazolinone and Quinazoline derivatives: Recent structures with potent antimicrobial and cytotoxic activities. Res. Pharm. Sci. 11 (2016) 1.
4. M.J Mphahlele, M.M Mmonwa, A. Aro, L.J McGaw, Y.S Choong, Synthesis, Biological Evaluation and Molecular Docking of Novel Indole-Aminoquinazoline Hybrids for Anticancer Properties. Int. J. Mol. Sci. 19 (2018) 2232.
5. T.S Patel, S..F Vanparia, U.H Patel, R.B Dixit, C.J Chudasama, B.D Patel, B.C Dixit, Novel 2, 3-disubstituted quinazoline-4(3*H*)-one molecules derived from amino acid linked

sulphonamide as a potent malarial antifolates for DHFR inhibition. Eur. J. Med. Chem. 129 (2017) 251–265.

6. Z. Wu, J. Zhang, J. Chen, J. Pan, L. Zhao, D. Liu, A. Zhang, J. Chen, D. Hu, B. Song, Design, synthesis, antiviral bioactivity and three-dimensional quantitative structure–activity relationship study of novel ferulic acid ester derivatives containing quinazoline moiety. Pest Manag. Sci. 73 (2017) 2079–2089.
7. B. Dash, S. Dash, D. Laloo, C. Medhi, Design, synthesis and preliminary pharmacological screening (antimicrobial, analgesic and anti-inflammatory activity) of some novel quinazoline derivatives. J. Appl. Pharm. Sci. **7 (**2017) 83–96.
8. G.F.S Fernandes, C. Man Chin, J.L Dos Santos, Advances in Drug Discovery of New Antitubercular Multidrug-Resistant compounds. Pharmaceuticals 10 (2017) 51.
9. S.L Mowbray, M.K Kathiravan, A.A Pandey, L.R Odell, Inhibition of Glutamine Synthetase: A Potential Drug Target in *Mycobacterium tuberculosis*. Molecules 19 (2014) 13161–13176.
10. P. Kosikowska, M. Bochno, K. Macegoniuk, G. Forlani, P. Kafarski, L. Berlicki, Bisphosphonic acids as effective inhibitors of *Mycobacterium tuberculosis* glutamine synthetase. J. Enzym. Inhib. Med. Chem. 31 (2016) 931–938.
11. J. Gising, M.T. Nilson, L.R. Odell, S. Yahiaoui, M. Lindh, H.Iyer, A.M. Sinha, B.R. Srinivasa, M. Larhed, S.L. Mowbray, A. Karlen. Trisubstituted imidazoles as *Mycobacterium tuberculosis* glutamine synthetase inhibitors. J. Med. Chem. 55 (2012) 2894 – 2898.
12. A. Nordqvist, M.T. Nilsson, O. Lagerlund, D. Muthas, J. Gising, S. Yahiaoui, L.R. Odell, B.R Srinivasa, M. Larhed, S.L. Mowbray, A. karlen. Synthesis, biological evaluation and X-

ray crystallographic studies of imidazo[1,2-a]pyridine-based *Mycobacterium tuberculosis* glutamine synthetase inhibitors. Med. Chem. Commun. 3 (2012) 620.

13. S. Parua, S. Das, R. Sikari, S. Sinha, N.D Paul, One-Pot Cascade Synthesis of Quinazolin-4-(3*H*)-ones via Nickel-Catalyzed Dehydrogenative Coupling of o-Aminobenzamides with Alcohols. J. Org. Chem. 82 (2017) 7165–7175.
14. N. Rahmannejadi, S. Khabnadideh, I. Yavari, Synthesis, docking, and cytotoxic activities of novel 2-aryl-4-(arylamino) quinazolines. Mon. Chem. Chem. Mon. 149 (2018) 2085–2092.
15. A.C Maxwell, S.P Flanagan, R. Goddard, P.J Guiry, Rhodium-catalysed hydroboration employing new Quinazolinap ligands; an investigation into electronic effects. Tetrahedron: Asymmetry 21 (2010) 1458–1473.
16. M.J Mphahlele, H.K Paumo, A.M El-Nahas, M.M El-Hendawy, Synthesis and Photophysical Property Studies of the 2,6,8-Triaryl-4-(phenylethynyl)quinazolines. Molecules 19 (2014) 795–818.
17. H.K Paumo, T.J Makhafola, M.J Mphahlele, Synthesis and In Vitro Cytotoxic Properties of Polycarbo-Substituted 4-(Arylamino) quinazolines. Molecules 21 (2016) 1366.
18. R. Chinchilla, C. Nájera, The Sonogashira reaction: A booming methodology in synthetic organic chemistry. Chem. Rev. 107 (2007) 874–922.
19. X. Wang, D. He, Y. Huang, Q. Fan, W. Wu, H. Jiang, Copper-Catalyzed Synthesis of Substituted Quinazolines from Benzonitriles and 2-Ethynylanilines via Carbon–Carbon Bond Cleavage Using Molecular Oxygen. J. Org. Chem. 83 (2018) 5458–5466.
20. C. Kieffer, P. Verhaeghe, N. Primas, C. Castera-Ducros, A. Gellis, R. Rosas, S. Rault, P. Rathelot, P. Vanelle, Sonogashira cross-coupling reaction in 4-chloro-2-

trichloromethylquinazoline series is possible despite a side dimerization reaction. Tetrahedron 69 (2013) 2987–2995.

21. X. Hu, B. Wan, Y. Liu, J. Shen, S.G Franzblau, T. Zhang, K. Ding, X. Lu, Identification of Pyrazolo [1,5-*a*] pyridine-3-carboxamide Diaryl Derivatives as Drug Resistant Anti-tuberculosis Agents. Am. Chem. Soc. Med. Chem. Lett. 10 (2019) 295–299.
22. P. Mishra, J. Albiol-Chiva, D. Bose, A. Durgbanshi, J. Peris-Vicente, S. Carda-Broch, J. Esteve-Romero, Optimization and Validation of a Chromatographic Method for the Quantification of Isoniazid in Urine of Tuberculosis Patients According to the European Medicines Agency Guideline. Antibiotics 7 (2018) 107.
23. R.V Chikhale, M.A Barmade, P.R Murumkar, M.R Yadav, Overview of the development of DprE1 inhibitors for combating the menace of tuberculosis. J. Med. Chem. 61 (2018) 8563–8593.
24. A.N Ambhore, S.S Kamble, S.N Kadam, R.D Kamble, M.J Hebade, S.V Hese, M.V Gaikwad, R.J Meshram, R.N Gacche, B.S Dawane, Design, synthesis and in silico study of pyridine based 1,3,4-oxadiazole embedded hydrazinecarbothioamide derivatives as potent anti-tubercular agent. Comput. Biol. Chem. 80 (2019) 54–65.
25. I. Orme, Search for new drugs for treatment of tuberculosis. Antimicrob. Agents Chemother. 45 (2001) 1943.
26. G.L Warren, C.W Andrews, A.M Capelli, B. Clarke, J. LaLonde, M.H Lambert, M. Lindvall, N. Nevins, S.F Semus, S. Senger, et al. A critical assessment of docking programs and scoring functions. J. Med. Chem. 46 (2006) 5912–5931.
27. E. Yuriev, M. Agostino, P.A Ramsland, Challenges and advances in computational docking: 2009 in review. J. Mol. Recognit. 24 (2011) 149–164.

28. A.P Graves, D.M Shivakumar, S.E Boyce, M.P Jacobson, D.A Case, B.K Shoichet, Rescoring docking hit lists for model cavity sites: Predictions and experimental testing. J. Mol. Biol. 377 (2008) 914–934.
29. D.L Mobley, K.A Dill, Binding of small-molecule ligands to proteins: "what you see" is not always "what you get". Structure 17 (2009) 489–498.
30. P.A Kollman, I. Massova, C. Reyes, B. Kuhn, S. Huo, L. Chong, M. Lee, T. Lee, Y. Duan, W. Wang, et al. Calculating structures and free energies of complex molecules: Combining molecular mechanics and continuum models. Acc. Chem. Res. 33 (2000) 889–897.
31. B. Kuhn, P.A Kollman, Binding of a diverse set of ligands to avidin and streptavidin: An accurate quantitative prediction of their relative affinities by a combination of molecular mechanics and continuum solvent models. J. Med. Chem. 43 (2000) 3786–3791.
32. D. Robinson, T. Bertrand, J.C Carry, F. Halley, A. Karlsson, M. Mathieu, H. Minoux, M.A Perrin, B. Robert, L. Schio, et al. Differential water thermodynamics determine PI3K-beta/delta selectivity for solvent-exposed ligand modifications. J. Chem. Inf. Model. 56 (2016) 886–894.
33. M. Ciordia, L. Pérez-Benito, F. Delgado, A.A Trabanco, G. Tresadern, Application of free energy perturbation for the design of BACE1 inhibitors. J. Chem. Inf. Model. 56 (2016) 1856–1871.
34. Schrödinger, LLC. Schrödinger Release 2018-3; QikProp: New York, NY, USA, 2018.
35. C.S de Melo, T.S Feng, R. van der Westhuyzen, R.K Gessner, L.J Street, G.L Morgans, D.F Warner, A. Moosa, K. Naran, N. Lawrence, et al. Aminopyrazolo [1,5-*a*] pyrimidines as potential inhibitors of Mycobacterium tuberculosis: Structure activity relationships and ADME characterization. Bioorg. Med. Chem. 23 (2015) 7240–7250.

36. Schrödinger, LLC. *Maestro*; Schrödinger, LLC: New York, NY, USA, 2018.
37. H.S Gill, D. Eisenberg, Crystallographic Structure of a Relaxed Glutamine Synthetase from Mycobacterium Tuberculosis. Available online: http://dx.doi.org/10.2210/pdb1hto/pdb (Accessed 10 March 2020).
38. Schrödinger, LLC. Schrödinger Release 2018-1: Schrödinger Suite 2018-1 Protein Preparation Wizard; Epik, Schrödinger, LLC: New York, NY, USA, 2018; Impact, Schrödinger, LLC: New York, NY, USA, 2018; Prime, Schrödinger, LLC: New York, NY, USA, 2018.
39. G.M Sastry, M. Adzhigirey, T. Day, R Annabhimoju, W Sherman, Protein and ligand preparation: Parameters, protocols, and influence on virtual screening enrichments. J. Comput. Aided Mol. Des. 27 (2013) 221–234.
40. Schrödinger, LLC. Schrödinger Release 2018-3; Prime: New York, NY, USA, 2018.
41. M.P Jacobson, D.L Pincus, C.S Rapp, T.J.F Day, B. Honig, D.E Shaw, R.A Friesner, A Hierarchical Approach to All-Atom Protein Loop Prediction. Proteins: Struct. Funct. Bioinform. 55 (2004) 351–367.
42. M.P Jacobson, R.A Friesner, Z. Xiang, B. Honig, On the Role of Crystal Packing Forces in Determining Protein Sidechain Conformations. J. Mol. Biol. 320 (2002) 597–608.
43. Schrödinger, LLC. Schrödinger Release 2018-1; Epik: New York, NY, USA, 2018.
44. J.R Greenwood, D. Calkins, A.P Sullivan, J.C Shelley, Towards the comprehensive, rapid, and accurate prediction of the favorable tautomeric states of drug-like molecules in aqueous solution. J. Comput. Aided Mol. Des. 24 (2010) 591–604.

884 45. J.C Shelley, A. Cholleti, L. Frye, J.R Greenwood, M.R Timlin, MM. Uchimaya, Epik: A
885 software program for pKa prediction and protonation state generation for drug-like
886 molecules. J. Comput. Aided Mol. Des. 21 (2007) 681–691.
887 46. C.R Sondergaard, M.H.M Olsson, M. Rostkowski, J.H Jensen, Improved Treatment of
888 Ligands and Coupling Effects in Empirical Calculation and Rationalization of pKa Values.
889 J. Chem. Theory Comput. 7 (2011) 2284−2295.
890 47. W.L Jorgensen, D.S Maxwell, J. Tirado-Rives, Development and Testing of the OPLS All-
891 Atom Force Field on Conformational Energetics and Properties of Organic Liquids. J. Am.
892 Chem. Soc. 118 (1996) 11225–11236.
893 48. W.L Jorgensen, J. Tirado-Rives, The OPLS [optimized potentials for liquid simulations]
894 potential functions for proteins, energy minimizations for crystals of cyclic peptides and
895 crambin. J. Am. Chem. Soc. 110 (1988) 1657–1666.
896 49. Schrödinger, LLC. Schrödinger Release 2018-1; LigPrep: New York, NY, USA, 2018.
897 50. Schrödinger, LLC. Schrödinger Release 2018-1: Schrödinger Suite 2018-1 Induced Fit
898 Docking Protocol; Glide: New York, NY, USA, 2018; Prime, Schrödinger, LLC: New York,
899 NY, USA, 2018.
900 51. R. Farid, T. Day, R.A Friesner, R.A Pearlstein, New insights about HERG blockade
901 obtained from protein modeling, potential energy mapping, and docking studies. Bioorg.
902 Med. Chem. 14 (2006) 3160–3173.
903 52. W. Sherman, T. Day, M.P Jacobson, R.A Friesner, R. Farid, Novel Procedure for Modeling
904 Ligand/Receptor Induced Fit Effects. J. Med. Chem. 49 (2006) 534–553.
905 53. W. Sherman, H.S Beard, R. Farid, Use of an Induced Fit Receptor Structure in Virtual
906 Screening. Chem. Biol. Drug Des. 67 (2006) 83–84.

54. Schrödinger, LLC. Schrödinger Release 2018-1; Glide: New York, NY, USA, 2018.
55. R.A Friesner, R.B Murphy, M.P Repasky, L.L Frye, J.R Greenwood, T.A Halgren, P.C Sanschagrin, D.T Mainz, Extra Precision Glide: Docking and Scoring Incorporating a Model of Hydrophobic Enclosure for Protein-Ligand Complexes. J. Med. Chem. 49 (2006) 6177–6196.
56. T.A Halgren, R.B Murphy, R.A Friesner, H.S Beard, L.L Frye, W.T Pollard, J.L Banks, Glide: A New Approach for Rapid, Accurate Docking and Scoring. 2. Enrichment Factors in Database Screening. J. Med. Chem. 47 (2004) 1750–1759.
57. R.A Friesner, J.L Banks, R.B Murphy, T.A Halgren, J.J Klicic, D.T Mainz, M.P Repasky, E.H Knoll, D.E Shaw, M. Shelley, et al. Glide: A New Approach for Rapid, Accurate Docking and Scoring. 1. Method and Assessment of Docking Accuracy. J. Med. Chem. 47 (2004) 1739–1749.
58. Bruker. *APEXII*; Bruker AXS Inc: Madison, WI, USA, 2009.
59. Bruker. *SAINT*; Bruker AXS Inc: Madison, WI, USA, 2009.
60. Bruker. *SADABS*; Bruker AXS Inc: Madison, WI, USA, 2009.
61. G.M Sheldrick, A short history of SHELX. Acta Crystallogr. Sect. A: Found. Crystallogr. 64 (2008) 112–122.
62. C.F. Macrae, I.J Bruno, J.A Chisholm, P.R Edgington, P. McCabe, E. Pidcock, L. Rodriguez-Monge, R. Taylor, J.V.D Streek, P.A Wood, Mercury CSD 2.0–new features for the visualization and investigation of crystal structures. J. Appl. Crystallogr. 41 (2008) 466–470.

929

930 **Graphical abstract**

931

932

933

934

935